



A model of early diagenetic processes from the shelf to abyssal depths

KARLINE SOETAERT, PETER M. J. HERMAN, and JACK J. MIDDELBURG

Netherlands Institute of Ecology, Centre for Estuarine and Coastal Ecology, Vierstraat 28, 4401 EA Yerseke, The Netherlands

(Received July 12, 1995; accepted in revised form December 18, 1995)

Abstract—We present a numerical model of sedimentary early diagenetic processes that includes oxic and anoxic mineralization. The model belongs to the new wave of early diagenesis models that account for depth-dependent bioturbation and porosity profiles; it can be used both for calculating steady-state conditions and transient simulation. It was developed to reproduce the cycling of carbon, oxygen, and nitrogen along the ocean margin; it resolves the sediment-depth profiles of carbon, oxygen, nitrate, ammonium, and other reduced substances.

Organic carbon is modeled as two degradable fractions with different first-order degradation rates and nitrogen:carbon ratios, to account for the decreasing reactivity and N/C ratio of the organic matter with depth into the sediment. The consumption of oxygen and nitrate as terminal electron acceptors is explicitly modeled, and mineralization is limited both by carbon (first order kinetics) and by oxidant availability (Michaelis-Menten type kinetics). Nitrification and oxic mineralization are decoupled, which allows the description of ammonium profiles. Mineralization processes using other oxidants (manganese oxides, iron oxides, sulphate) are lumped into one process, where degradation is only carbon limited; the terminal electron acceptors are not explicitly modeled, only the production of reduced substances is described. These substances are in part permanently removed (e.g., pyrite formation below the bioturbation zone) and partly diffuse towards the oxic layer where they react with oxygen.

The values of several parameters were constrained using literature-derived relationships. The model was calibrated on a dataset obtained from the literature, which relates the magnitude of the different pathways to total organic carbon mineralization. The influence of carbon flux, bioturbation, sedimentation rate, bottomwater concentrations of oxygen, and nitrate and carbon degradability on the different mineralization pathways is examined. The relative contribution of the oxic mineralization in the model is significantly depressed under high organic flux, under low bottomwater oxygen conditions and when the bioturbation increases; higher carbon degradability has only a small positive effect, while sedimentation rate is relatively unimportant. Denitrification is mainly influenced by the nitrate concentration in the overlying bottomwater.

1. INTRODUCTION

When organic carbon settles on the seafloor, it may either become (permanently) buried or it may provoke a sequence of degradation reactions that remove carbon from the sediment system (by oxidizing it to CO_2). There exists a well-defined sequence in the use and exhaustion of terminal electron acceptors, because the energy gained through mineralization differs with the nature of these oxidants and/or they are mutually exclusive. Oxygen (the most powerful oxidant) will be consumed first, followed by nitrate and nitrite, manganese oxide, iron oxides, sulfate, and finally oxygen bound in organic matter (Froelich et al., 1979).

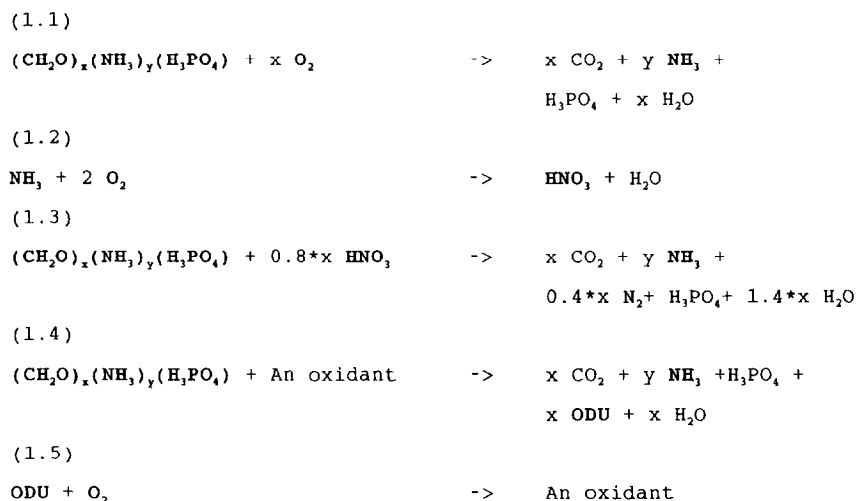
In the deep sea, where organic matter deposition is low, oxygen is by far the major electron acceptor in the mineralization process (Jahnke et al., 1982; Goloway and Bender, 1982; Heggie et al., 1987) and almost no carbon escapes the zone of oxic mineralization. With increasing organic deposition, suboxic and anoxic processes become more important and in shelf sediments sulphate reduction can account for more than half of the total mineralization (Jørgensen, 1983; Canfield, 1993).

Depth in the sediment can be considered as a measure of time since deposition. Hence, the succession in mineralization pathways translates into clear vertical gradients of both the oxidants and products of the degradation process (Berner,

1980a). As these porewater profiles are sensitive indicators of organic matter degradation (Jahnke et al., 1982), they can be used to derive certain properties of the mineralization process, e.g., the amount of carbon degraded, the mineralization rates, the relative importance of the different pathways, etc. Interpretation of these biogeochemical patterns is frequently done with models which incorporate both physical processes (transport) and biochemical reactions. As many of these models are restricted to a few biochemical reactions, they are only applicable to specific types of sediments, e.g., deep-sea sediments (Jahnke et al., 1982; Heggie et al., 1987; Goloway and Bender, 1982; Rabouille and Gaillard, 1991a), or they provide only information on a subset of mineralization processes that occur in sediments (e.g., manganese reduction Gratton et al., 1990). Other models include more biochemical reactions and the associated coupling between chemical species (Rabouille and Gaillard, 1991b; Aller, 1990).

Except for the most organic-poor deep-sea sediments, a substantial fraction of the total oxygen consumption can be used for the reoxidation of reduced products originating from anaerobic mineralization (Aller, 1990; Boudreau and Canfield, 1993). Hence, one usually cannot ignore the processes that occur in the anaerobic zone of the sediments. Nevertheless, there are only a few models that include descriptions of both oxic and anoxic mineralization. Aller (1990) devised

Table 1. Idealized diagenetic reactions used in the model. In bold are components that are modeled. y denotes the molar N:P ratio, x the molar C:P ratio in organic matter per mole of phosphorus (for Redfield Stoichiometry, $x=106$, $y = 16$). ODU stands for oxygen demand units.



an analytical model that incorporated degradation by oxygen, nitrate, and manganese oxides and accounted for the reoxidation of reduced manganese and ammonium. Boudreau and Canfield (1993) developed a pH model that incorporated sequential oxidation of organic matter by oxygen, nitrate, and sulphate. Ditoro et al. (1990) devised an analytical model of sediment oxygen demand, applicable for lake and stream sediments, which included the oxidation of dissolved methane and ammonium. The model of Rabouille and Gaillard (1991b) included reoxidation of reduced manganese, but did not consider ammonium or other reduced substances. In three very recent papers, to which our attention was drawn during review, Dhakar and Burdige (1996), Van Cappellen and Wang (1995), and Boudreau (1995) have presented coupled numerical models that include reoxidation kinetics for early diagenetic process reactions.

In this manuscript we present a coupled, nonlinear, general diagenetic model that incorporates oxic mineralization, denitrification, anoxic mineralization (including Mn, Fe, SO_4 consumption), and the oxidation of ammonium (nitrification) and other reduced compounds. The model has primarily been developed (1) to examine the cycling of carbon, oxygen, and nitrogen along sedimentary gradients such as the ocean margin and (2) to allow coupling to/with water column carbon, oxygen, and nitrogen cycling models. Any diagenetic model to be coupled to biogeochemical ocean models should be simple, the number of unknown or poorly constrained parameters should be reduced and computing time minimized. Yet the model should be sufficiently elaborate to accurately calculate the distribution of compounds of interest.

During model development, emphasis has been given to reproducing observed trends along sedimentary gradients rather than accurate replication of measured concentration

profiles at a selected station. In order to reduce the number of model parameters, we constrain most of them using relationships derived from the literature. The remaining parameters, mainly relating to microbial processes are derived during calibration. It appears that the model parameters are either predictable or constant at a global scale, which is a prerequisite for application of diagenetic models along the ocean margin.

The model resolves the gradients of oxygen, nitrate, ammonium, carbon, and reduced substances formed during anoxic mineralization. Profiles of manganese, iron, and sulphur compounds are not generated and as such the model cannot be used to examine the importance of the manganese or iron pathways in organic matter decomposition. The numerical scheme we propose has been checked against well-known analytical solutions, and the advective-diffusive approximation precludes any numerical loss of substance.

Recently, Tromp et al. (1995) also presented a model for early diagenesis that can be applied at a global scale. However, their model is less general, given its layered nature, the use of first-order kinetics for organic matter decomposition, and that it does not explicitly include reoxidation processes. Moreover, Tromp et al. (1995) have focussed on carbon and phosphorus, whereas our model primarily addresses the cycling of carbon, oxygen, and nitrogen.

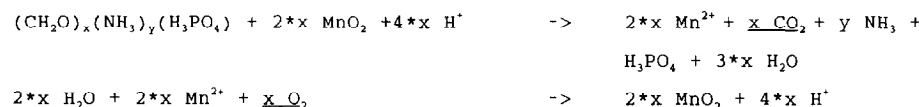
2. BIOCHEMICAL REACTIONS

The idealized reactions that influence the distribution of the porewater species and of the organic matter are represented in Tables 1 and 2 and in Fig. 1. The stoichiometry of the organic matter is represented by the coefficients x (denoting the molar C:P ratio) and y (denoting the molar N:P ratio).

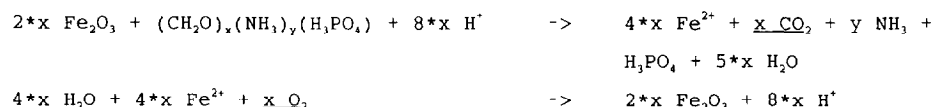
Table 2. Idealized diagenetic reactions that are lumped in the model

(giving rise to eqs. 1.4, 1.5 in table 1). Underlined is the amount of CO₂ produced and the amount of O₂ needed to oxidize the reduced substance. Symbols as in table 1.

(2.1)



(2.2)



(2.3)



As we are mainly interested in modeling carbon, oxygen, and nitrogen along a sedimentary gradient, we explicitly include organic carbon, oxygen, nitrate, and ammonium in our model, while the other reduced compounds are lumped together. This diminishes both the model complexity and the calculation time, at the expense of little loss in predictive power.

Oxic carbon mineralization produces ammonium (Table 1, Eqn. 1.1), which is further oxidized to nitrate (nitrification, Table 1, Eqn. 1.2). Nitrate-based mineralization (denitrification, Table 1, Eqn. 1.3) produces ammonium and nitrogen gas; the latter is lost from the sediment and is not modeled. The other diagenetic reactions involving manganese, iron, and sulfate are represented in Table 2. These reactions produce ammonium and some reduced substance. Complete re-oxidation of this reduced substance, formed through the oxidation of x moles of carbon, requires x moles of oxygen, whatever the anoxic pathway considered (Table 2, Eqns. 2.1–2.3). Hence, instead of modeling each of these processes separately, they can be lumped together (Table 1, Eqns. 1.4–1.5). In what follows, this process is termed “anoxic mineralization.” Anoxic mineralization of 1 mole of carbon produces 1 mole of an apparent oxygen demand unit (hereafter termed ODU; Table 1, Eqn. 1.4). Reoxidation of one mole of ODU requires one mole of oxygen (Table 1, Eqn. 1.5). We did not include methane formation in Table 2, because this process is not important along the ocean margin (Canfield, 1993), but here too the same amount of ODUs would be formed.

In order to incorporate the coupling between nitrification and denitrification and to distinguish between the various oxygen consumption processes, our model reactions are somewhat different from those given by Froelich et

al. (1979) and Emerson et al. (1980), where only N₂ is formed through the process of manganese reduction, and from those used by Bender et al. (1989) and Aller (1990), who consider oxidation of ammonium coupled to reduction of nitrate.

3. MODEL EQUATIONS

3.1. Description

The model equations that describe the processes in Table 1 are given in Table 3; state variables and their units are found in Table 4 and a description of intermediate variables and parameters is given in Tables 5 and 6. There is a large discrepancy between the turnover times of, e.g., oxygen (on the order of seconds or minutes) and of carbon (on the order of years, Jørgensen, 1983). As the model must be able to resolve both timescales, and as we are mainly interested in seasonal variations, we expressed the model's rates in days.

3.2. Reactivity of Carbon

Following deposition, the organic substrates are sequentially consumed according to their decreasing lability. As a result the reactivity of organic matter decreases with time during mineralization (Jørgensen, 1978; Berner, 1980b; Westrich and Berner, 1984; Middelburg, 1989). Several models have been developed to represent this decreasing mean degradability with age of the carbon. The most recent ones (Middelburg, 1989; Boudreau and Ruddick, 1991) regard organic matter as consisting of a continuum of fractions with different degradabilities, in contrast to the multi-G class of models (Westrich and Berner, 1984), in which a finite

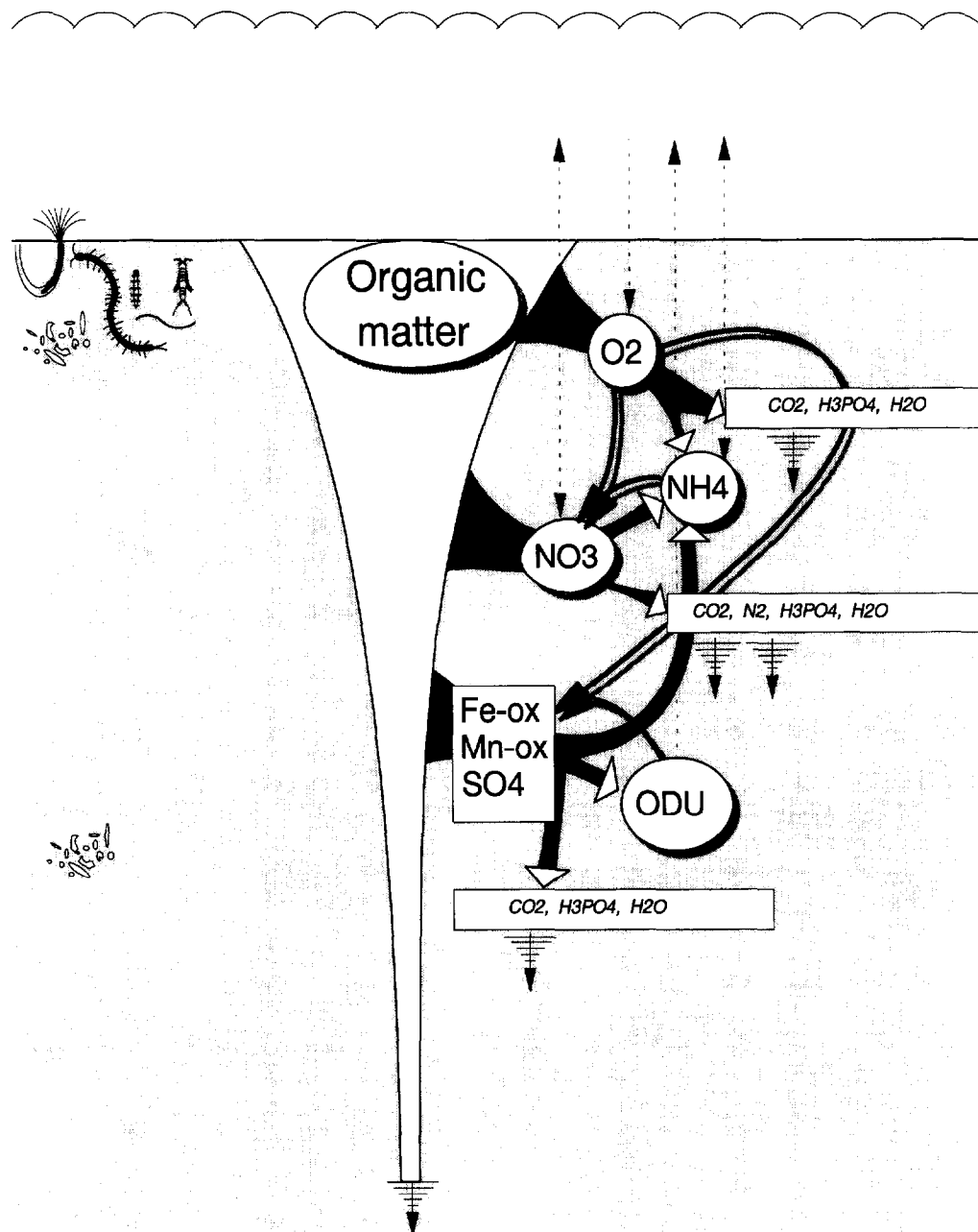


Fig. 1. Schematic representation of the modeled early diagenetic processes. Circles indicate those substances whose concentrations are modeled. Nutrients represented in the rectangle are not explicitly modeled, but the anoxic mineralization is represented by the formation of reduced substances (Oxygen Demand Units, ODU). Solid arrows represent the reoxidation processes, dashed arrows represent sediment-water exchange, cross-hatched arrows indicate losses to the system (gas escape or permanent burial).

number of degradable fractions with fixed mineralization rates is considered. Although conceptually superior, the "continuum" models are not easily applied to sedimentary systems. Van Cappellen et al. (1993) attempted to incorporate the power model of Middelburg (1989) in a diagenetic model, by linking the degree of advancement of the degradation process (i.e., the "age") to the total amount of carbon already consumed. However, their method, which uses the relative proportion of the carbon flux across sediment layers versus the flux at the sediment-water interface, is only appli-

cable in steady-state flux conditions. Consequently, we resort to the multi-G class of models (Westrich and Berner, 1984) because they are easily incorporated into nonsteady-state models.

Three different classes of carbon are considered. The "refractory" carbon (i.e., the carbon whose degradability is not relevant for the timescales considered) is not modeled, but its concentration can be calculated (see below). Additionally, two degradable fractions have fixed first-order degradation constants (day^{-1}) that span two orders of magnitude. As the

Table 3. Biochemical model formulations, described in each sediment layer:

$$(3.1) \quad OxicMin_i = R_{Miner_i} * \frac{O_2}{O_2 + K_{s_{O_2}}} * TOC_i * \frac{1}{\Sigma \lim}$$

$$(3.2) \quad Denit_i = R_{Miner_i} * \frac{NO_3}{NO_3 + K_{s_{NO_3}}} * (1 - \frac{O_2}{O_2 + K_{in_{O_2}^{Denit}}}) * TOC_i * \frac{1}{\Sigma \lim}$$

$$(3.3) \quad AnoxMin_i = R_{Miner_i} * (1 - \frac{NO_3}{NO_3 + K_{in_{NO_3}^{AnoxMin}}}) * (1 - \frac{O_2}{O_2 + K_{in_{O_2}^{AnoxMin}}}) * TOC_i * \frac{1}{\Sigma \lim}$$

for $i=1,2$ (one of the degradable fractions)

$$(3.4) \quad \Sigma \lim = \frac{O_2}{O_2 + K_{s_{O_2}}} + \frac{NO_3}{NO_3 + K_{s_{NO_3}}} * (1 - \frac{O_2}{O_2 + K_{in_{O_2}^{Denit}}}) + (1 - \frac{NO_3}{NO_3 + K_{in_{NO_3}^{AnoxMin}}}) * (1 - \frac{O_2}{O_2 + K_{in_{O_2}^{AnoxMin}}})$$

$$(3.5) \quad SolidODU = R_{solid} * [AnoxMin_1 + AnoxMin_2] * \gamma_{TOC}^{ODU} * \frac{1-\Phi}{\Phi}$$

$$(3.6) \quad ODU_{oxid} = R_{ODU_{ox}} * ODU * \frac{O_2}{O_2 + K_{s_{ODU_{ox}}}}$$

$$(3.7) \quad NH_3_{oxid} = R_{nitrif} * NH_3 * \frac{O_2}{O_2 + K_{s_{Nitrif}}} + [OxicMin_1 * \gamma_{TOC1}^N + OxicMin_2 * \gamma_{TOC2}^N] * \frac{(1-\Phi)}{\Phi}$$

Summing up:

$$(3.8) \quad \frac{dTOC_i}{dt} = @ - OxicMin_i - Denit_i - AnoxMin_i \quad (= @ - R_{Miner_i} * TOC_i)$$

for $i=1,2$

$$(3.9) \quad \frac{dODU}{dt} = @ + [AnoxMin_1 + AnoxMin_2] * \gamma_{TOC}^{ODU} * \frac{1-\Phi}{\Phi} - ODU_{oxid} - SolidODU$$

$$(3.10) \quad \frac{dO_2}{dt} = @ - [OxicMin_1 + OxicMin_2] * \gamma_{TOC}^{O_2} * \frac{1-\Phi}{\Phi} - ODU_{oxid} - NH_3_{oxid} * \gamma_{NH_3}^{O_2}$$

$$(3.11) \quad \frac{dNO_3}{dt} = @ - [Denit_1 + Denit_2] * \gamma_{TOC}^{NO_3} * \frac{1-\Phi}{\Phi} + NH_3_{oxid}$$

$$(3.12) \quad \frac{dNH_3}{dt} = @ + \frac{[OxicMin_1 + Denit_1 + AnoxMin_1] * \gamma_{TOC1}^N + [OxicMin_2 + Denit_2 + AnoxMin_2] * \gamma_{TOC2}^N}{1 + NH_3_{ads}} * \frac{1-\Phi}{\Phi} - \frac{NH_3_{oxid}}{1 + NH_3_{ads}}$$

where @ denotes all transport processes.

more degradable carbon is decomposed at a much faster rate, the relative concentration of both fractions changes with time, thus imitating decreasing reactivity of the total carbon pool. Furthermore, we assume that the most degradable frac-

tion has Redfield stoichiometry, while the least degradable fraction is poorer in nitrogen. This mimics the increasing carbon to nitrogen ratio with depth into the sediment (Jørgensen, 1983; Burdige, 1991).

Table 4. State variables modeled:

NAME	UNITS	DESCRIPTION
TOC ₁ , TOC ₂	μmol.l ⁻¹ solid	Concentration of fast, respectively slow decay carbon.
O ₂	μmol.l ⁻¹ liquid	Concentration of oxygen
NO ₃	μmol.l ⁻¹ liquid	Concentration of nitrate (+nitrite)
NH ₃	μmol.l ⁻¹ liquid	Concentration of ammonium
ODU	μmol.l ⁻¹ liquid	Concentration of oxygen demand units (=the amount of O ₂ necessary to reoxidize).

Table 5. Variables used in the biochemical part of the model.

NAME	UNITS	DESCRIPTION
OxicMin ₁	$\mu\text{mol C.l}^{-1} \text{ solid.d}^{-1}$	the amount of carbon oxidized by O ₂
Denit	$\mu\text{mol C.l}^{-1} \text{ solid.d}^{-1}$	the amount of carbon oxidized by NO ₃
AnoxMin	$\mu\text{mol C.l}^{-1} \text{ solid.d}^{-1}$	the amount of carbon oxidized by other oxidants
SolidODU	$\mu\text{mol O}_2.\text{l}^{-1} \text{ liquid.d}^{-1}$	the amount of ODU deposited as solids (expressed in O ₂ -equivalents).
ODUoxid	$\mu\text{mol O}_2.\text{l}^{-1} \text{ liquid.d}^{-1}$	the amount of O ₂ consumed in the oxidation of reduced substances
NH ₃ oxid	$\mu\text{mol O}_2.\text{l}^{-1} \text{ liquid.d}^{-1}$	the amount of NH ₃ nitrified

3.3. Limitation and Inhibition Functions

The rate of metabolic activity depends not only on the degradability of the organic matter, but also on the availability of the oxidant utilized. This oxidant limitation is represented by a hyperbolic function (Monod or Michaelis-Menten type) with a half-saturation constant K_s (e.g., 2nd term in Eqn. 3.1 of Table 3). If the limiting substance has a concentration K_s , the process proceeds at half the maximal speed; as the concentration increases, the limitation becomes weaker (or the value of the limitation function increases) and the metabolic rate will increase.

The presence of some oxidants may inhibit other metabolic pathways. Inhibition by some oxidant is represented as one minus a hyperbolic function, with a half-saturation constant K_{in} (e.g., 3rd term in Eqn. 3.2 of Table 3). This is equivalent to the inhibition function suggested by Van Cappellen et al. (1993) (citing Humphrey, 1972). The process proceeds at half the maximal speed if the concentration of the inhibiting substance equals the half-saturation constant. As the concentration of inhibitory substance increases, inhibition becomes stronger (or the value of the inhibition function decreases) and the observed rate decreases.

The use of limiting and inhibitory functions in our numerical model allows us to use a single equation for each component over the entire model depth and provides a direct coupling between the various substances.

3.4. Process Descriptions

Oxic degradation of the two carbon fractions is limited by oxygen (Table 3, Eqn. 3.1). Denitrification is limited by nitrate concentration and is inhibited by oxygen (Table 3, Eqn. 3.2); anoxic mineralization processes are not limited by any oxidant, but they are inhibited by nitrate and oxygen concentrations (Table 3, Eqn. 3.3). All metabolic processes are first-order with respect to the organic carbon fraction (i.e., the rate is proportional to the carbon concentration). It is assumed that the maximal degradation rate is the same for the different mineralization pathways.

Because the anoxic degradation is unlimited by the reactants (which are not modeled), mineralization proceeds until all degradable carbon is removed. As the different competing mineralization pathways can occur simultaneously and the limitation and inhibition functions are independently calculated, the functions are rescaled (Table 3, Eqn. 3.4) to ensure that the maximum degradation rate is always achieved. Without this rescaling procedure, the total attained mineralization rate in some sediment layer could be up to 7% higher than the "maximum" degradation rate. By allowing the organic matter to undergo decomposition at a rate which is primarily independent of the various electron acceptors, the organic carbon distribution can be solved independently from the distribution of the porewater species, used or produced in the degradation of organic matter.

Table 6. Parameters used in the biochemical part of the model

(*) indicates that they are calculated, parameter values in bold were obtained by calibration; the others were either obtained from the literature or they were fixed through the stoichiometry of the biochemical reactions.

NAME	UNITS	VALUE	DESCRIPTION
$R_{\text{Miner}1,2}$	d^{-1}	(*)	Maximum degradation rate of the organic carbon fraction
K_{SO_2}	$\mu\text{mol O}_2.\text{l}^{-1}$	3	Half-saturation const for O ₂ limitation in oxic mineralization
K_{SNO_3}	$\mu\text{mol NO}_3.\text{l}^{-1}$	30	Half-saturation const for NO ₃ limitation in denitrification.
$K_{\text{in}}^{\text{Denit}}$	$\mu\text{mol O}_2.\text{l}^{-1}$	10	Half-saturation const for O ₂ inhibition in denitrification.
$K_{\text{in}}^{\text{Anox Min NO}_3}$	$\mu\text{mol NO}_3.\text{l}^{-1}$	5	Half-saturation const for NO ₃ inhibition in anoxic mineralization
$K_{\text{in}}^{\text{Anox Min O}_2}$	$\mu\text{mol O}_2.\text{l}^{-1}$	5	Half-saturation const for O ₂ inhibition in anoxic mineralization
R_{solid}	d^{-1}	(*)	Part of ODU production that is deposited as a solid per day
$K_{\text{SMiner}1,2}$	$\mu\text{mol O}_2.\text{l}^{-1}$	1	Half-saturation const for O ₂ limitation in nitrification.
$K_{\text{SODUox nutrients}}$	$\mu\text{mol O}_2.\text{l}^{-1}$	1	Half-saturation const for O ₂ limitation in oxidation of reduced
R_{ODUox}	d^{-1}	20	Maximum oxidation rate of Oxygen Demand Units
R_{Nitrif}	d^{-1}	20	Maximum nitrification rate
$Y_{\text{OC}}^{\text{ODU}}$	$\text{mol O}_2.(\text{mol C})^{-1}$	1	Mol ODU formed per mol C in anoxic mineralization
$Y_{\text{OC}}^{\text{O}_2}$	$\text{mol O}_2.(\text{mol C})^{-1}$	1	Mol O ₂ used per mol C in oxic mineralization
$Y_{\text{OC}}^{\text{NO}_3}$	$\text{mol NO}_3.(\text{mol C})^{-1}$	0.8	Mol NO ₃ used per mol C in denitrification
$Y_{\text{OC}1}^{\text{N}}$	$\text{mol N.}(\text{mol C})^{-1}$	0.1509	N-C ratio of fast decay detritus
$Y_{\text{OC}2}^{\text{N}}$	$\text{mol N.}(\text{mol C})^{-1}$	0.1333	N-C ratio of slow decay detritus
$Y_{\text{NH}_3}^{\text{O}_2}$	$\text{mol O}_2.(\text{mol NH}_3)^{-1}$	2	Mol O ₂ needed to oxidize one mol of NH ₃ in nitrification
NH ₃ ads	-	1.3	Adsorption coefficient of ammonium
ϕ	-	(*)	porosity of the sediment (volume of liquid per volume of bulk sediment)

Part of the reduced substances that are produced through anoxic mineralization (the oxygen demand units, ODU) are permanently lost from the system (Table 3, Eqn. 3.5) as they are deposited as solid substances, such as pyrite (Berner, 1970) and manganese carbonate (Pedersen and Price, 1982) below the zone of bioturbation. The oxidation of the oxygen demand units (Table 3, Eqn. 3.6) and of ammonium (nitrification, Table 3, Eqn. 3.7) is limited by the oxygen concentration. It is assumed that ammonium formed in the oxic mineralization process is instantaneously oxidized by oxygen (for consistency with most earlier models). Although both oxidation processes can occur chemosynthetically, the amount of CO₂ incorporated into biomass by chemosynthetic bacteria is very low and autotrophic carbon production is relatively unimportant (Rowe and Staresinic, 1979; Jørgensen, 1983) and, hence, not modeled here.

The coupling of all the processes takes into account the conversion from solid to liquid units (when necessary) and the stoichiometric conversion factors that are determined by the biochemical reactions (Table 3, Eqns. 3.8–3.12). For ammonium, adsorption is taken into account (Berner, 1980a; see Appendix A1).

4. TRANSPORT EQUATIONS

Apart from biogeochemical reactions, the concentration vs. depth profiles of solids and/or liquids are also influenced by bioturbation, sediment deposition and compaction, and molecular and biologically enhanced diffusion. The general transport equation used is given in Appendix A1; boundary conditions can be found in Appendix A2. The model resolves only vertical gradients; it is assumed that horizontal variations are negligible. Bioturbation is modeled as a local transport process, analogous to eddy diffusion, and does not mix fluids against solids (i.e., intraphase mixing, Boudreau, 1986).

For the porewater solutes, the fluxes across the sediment-water interface are driven by an imposed bottomwater concentration; the numerical schematization at the interface takes into account the presence of a diffusive boundary layer (see below); the lower boundary satisfies a no-gradient condition. For carbon, a flux at the sediment-water interface is imposed, while at the lower limit, the concentrations of both degradable fractions are zero.

Because of the nonlinear kinetics (Monod) and the use of spatially variable porosity and bioturbation profiles (see below), and because of our intention to use the model in different nonsteady-state simulations, an analytical solution to the system of differential equations was not feasible and it is approximated by a system of numerical equations.

The derivation of the numerical scheme for the transport equations is given in Appendix A3. Care was taken to conserve mass fully, even for sharp gradients in porosity or particle mixing coefficients. The accuracy of the numerical scheme was tested using well-known analytical solutions (for constant porosity and bioturbation and using simple first-order decay) described in Van Genuchten (1981: his case A2, B2). Accuracy depended mostly on the thickness of the uppermost layer: the thinner this layer, the closer the numerical solution was to the analytical solution (not de-

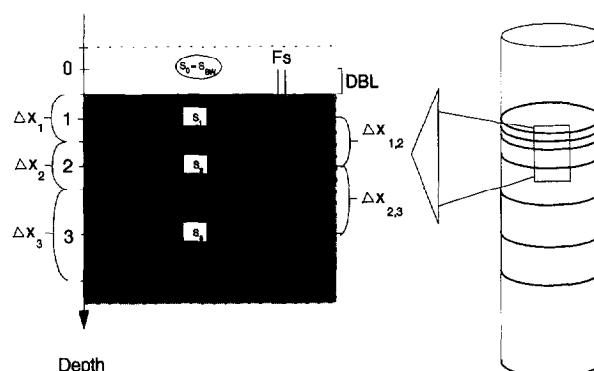


Fig. 2. Numerical scheme used in the model. s_i = concentration of the modeled substance, F_s is the flux, DBL stands for diffusive boundary layer.

picted). A thickness of the first layer of 1 mm provided good accuracy for solids with first-order decay of .05 d⁻¹ (18 y⁻¹, which is higher than the rate of the most degradable fraction in the model). One then assumes that the sedimenting carbon is instantaneously mixed within this 1 mm thick layer. Furthermore, a 1 mm thick layer implies that the diffusive boundary layer is 0.5 mm thick (Fig. 2), which is close to values reported from deep-sea sediments and along the shelf (Reimers et al., 1992; Archer and Devol, 1992). As using 1 mm slices throughout would result in a too large set of equations, the sediment column was subdivided into unequally spaced layers: the two uppermost layers 0.1 cm thick, the third layer 0.2 cm thick, the remaining layers 0.4 cm thick (Fig. 2).

Porosity usually declines with depth into the sediment (Jahnke et al., 1986) and is described by an equation of the form (Rabouille and Gaillard, 1991a; Berner, 1980a; Fig. 3)

$$\Phi_x = \Phi_\infty + (\Phi_0 - \Phi_\infty) * e^{-(x/\text{coeff}_\Phi)}$$

The diffusion coefficient of a dissolved substance in the sediment at ambient temperature T can be calculated from porosity (Φ) and sediment resistivity (F) as

$$D_s^T = \frac{D^T}{\Phi F},$$

where D^T is the diffusion coefficient in a free solution at $T^\circ\text{C}$. According to Ullman and Aller (1982), F relates to porosity as

$$\frac{1}{F} = \Phi^m$$

in which m varies from 2.5 to 3 in nearshore muds. A similar relationship was found for high porosity offshore muds by Reimers et al. (1992).

Setting $m = 3$, the diffusion coefficient in the sediment D_s^T is calculated as (Fig. 3)

$$D_s^T = D^T \Phi^2.$$

The free-solution diffusion coefficient at the ambient temper-

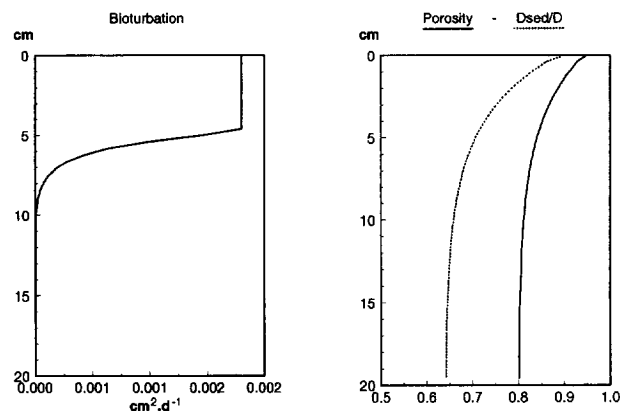


Fig. 3. Bioturbation, porosity profiles, and the ratio of the sediment diffusion coefficient and the free-solution diffusion coefficient used in the model.

ature (T) is calculated from the zero-degree coefficient D^0 as

$$D^T = D^0 + aT,$$

where a is an ion-specific coefficient. Values for D^0 were obtained from Li and Gregory (1974). Values for a were obtained by linearly interpolating between the diffusion coefficient at 0°C and at 18°C (Li and Gregory, 1974) (see Table 7). For the oxygen demand units, we used the diffusion coefficient of HS^- .

Bioturbation is assumed to be constant in a layer with thickness x_b and subsequently declines rapidly (Fig. 3). Thus, for $x \leq x_b$,

$$Db_x = Db_0,$$

below which ($x > x_b$)

$$Db_x = Db_0 * e^{[-(x-x_b)/\text{coeffDb}]},$$

We used the (somewhat arbitrary) value of 5 cm for the "constant mixed layer" and a value of 1 for the exponential coefficient (see Table 7). As such, bioturbation approaches

zero at about 10 cm depth (Fig. 3), which is consistent with values cited in Boudreau (1994).

5. MODEL IMPLEMENTATION

The model first calculates the steady-state profiles, after which a transient simulation can be run under time-variable forcing, using the steady-state concentration profiles as a starting condition. These time-dynamic simulations are not discussed in this paper, but in Soetaert et al. (1996).

For the calculation of the steady-state profiles, a set of nonlinear, strongly coupled differential equations has to be solved (the equations of Table 3 and from Appendix A3, with the rates of change dS/dt and dC/dt set to 0). The transport and reaction equations were solved together. Starting from a crude order-of-magnitude guess of the various concentrations, this set is solved using an iterative numerical root-finding technique (the Newton-Raphson method, Press et al., 1987). In a first step the equations relating to the two carbon fractions are solved (they are unaffected by the other profiles). Then the set relating to the oxygen, nitrate, ammo-

Table 7. Parameters used in the transport equations of the model. Values indicated as (*) were allowed to vary.

NAME	UNITS	VALUE	DESCRIPTION
Φ_0	-	0.95	Porosity at the sediment-water interface.
Φ_∞	-	0.8	Porosity at infinite sediment depth.
Coeff Φ	cm	4	Coefficient for exponential porosity change.
x_b	cm	5	Depth below which bioturbation decreases exponentially.
coeffDb	cm	1	Coefficient for exponential bioturbation decrease.
$D_{\text{NO}_3}^{0^\circ\text{C}}$	$\text{cm}^2 \cdot \text{d}^{-1}$	0.845	Molecular diffusion coefficient of Nitrate at 0°C.
a_{NO_3}	$\text{cm}^2 \cdot \text{d}^{-1} \cdot (^\circ\text{C})^{-1}$	0.0336	Coefficient for temperature dependency of diffusion coeff. of NO_3 .
$D_{\text{NH}_4}^{0^\circ\text{C}}$	$\text{cm}^2 \cdot \text{d}^{-1}$	0.847	Molecular diffusion coefficient of Ammonium at 0°C.
a_{NH_4}	$\text{cm}^2 \cdot \text{d}^{-1} \cdot (^\circ\text{C})^{-1}$	0.0336	Coefficient for temperature dependency of diffusion coeff. of NH_4 .
$D_{\text{O}_2}^{0^\circ\text{C}}$	$\text{cm}^2 \cdot \text{d}^{-1}$	0.955	Molecular diffusion coefficient of Oxygen at 0°C.
a_{O_2}	$\text{cm}^2 \cdot \text{d}^{-1} \cdot (^\circ\text{C})^{-1}$	0.0386	Coefficient for temperature dependency of diffusion coeff. of O_2 .
$D_{\text{ODU}}^{0^\circ\text{C}}$	$\text{cm}^2 \cdot \text{d}^{-1}$	0.842	Molecular diffusion coefficient of HS^- at 0°C.
a_{ODU}	$\text{cm}^2 \cdot \text{d}^{-1} \cdot (^\circ\text{C})^{-1}$	0.0242	Coefficient for temperature dependency of diffusion coeff. of HS^- .
NO_3BW	$\mu\text{mol} \cdot \text{l}^{-1}$	(*)	Nitrate concentration of the overlying water
O_2BW	$\mu\text{mol} \cdot \text{l}^{-1}$	(*)	Oxygen concentration of the overlying water
NH_4BW	$\mu\text{mol} \cdot \text{l}^{-1}$	0	Ammonium concentration of the overlying water
ODUBW	$\mu\text{mol} \cdot \text{l}^{-1}$	0	ODU concentration of the overlying water

nium, and ODU profile is solved. Both sets normally required less than ten iterations.

Limits on the minimum modeled sediment depth were set by the boundary conditions at the lower boundary which require the absence of gradients (see Appendix A2). In practice, this means that all degradable carbon had to be consumed within the modeled sediment column. As the thickness of the sediment layer at the interface was fixed to 1 mm, increasing the sediment depth was achieved by increasing the number of modeled segments. For most model runs, a thickness of about 20 cm was sufficient (equivalent to 50 model compartments). For the shallowest station (100 m), 100 model compartments (40 cm) were necessary. Convergence of the model was tested by computing the residuals to the differential equations for each sediment layer. Mass conservation for all compounds was better than 99.999%.

The model was implemented into the (dynamic) simulation environment SENECA (De Hoop et al., 1993) on a personal computer (66 mHz).

6. CALIBRATION

Model calibration proceeded by adjusting unknown parameter values so as to reproduce carbon and nitrogen mineralization rates in marine sediments from the shelf to the abyssal depths reported in the literature. Our calibration exercise was not aimed at providing the best fits to concentration versus depth profiles for a specific station. Nevertheless, care was taken to yield concentration profiles that mimic those reported in the literature.

We constrained the model as much as possible by imposing chosen relationships between variables. We used water depth as the “master variable,” based on which we calculated the first-order degradation rates and the proportion of the two metabolizable carbon fractions, the mean sedimentation rate, and the temperature. The value of the sedimentation rate was then used to fix the total flux of mineralizable and of refractory carbon, the bioturbation coefficient, and the rate of solid deposition. The literature data on which these regressions were based are gathered in Table 8.

The only remaining unknowns were the inhibition and limitation factors.

6.1. Defining Relationships Between Model Parameters

6.1.1. Water depth and sedimentation rate

Sedimentation rates (w , in $\text{cm} \cdot \text{y}^{-1}$) generally decrease with water depth (D , in m), although there is considerable variability, spanning at least two orders of magnitude. At depths less than 100 m, sedimentation rates seem to be less predictable or at least lower than expected. As these shallow sediments do not fit in the scope of this study, these values were not considered in the regression. The regression obtained (for $D > 100$ m) is (Fig. 4a; $r^2 = 0.66$, $N = 110$)

$$w = 982D^{-1.548}.$$

6.1.2. Sedimentation rate and the amount of organic carbon metabolized

The relationship between sedimentation rate and the total amount of carbon that is mineralized in the sediment is given by the power function ($r^2 = 0.63$, $N = 55$)

$$C_{\text{min}} = 0.59w^{0.58},$$

where C_{min} is in $\text{mM} \cdot \text{cm}^{-2} \cdot \text{yr}^{-1}$ and w is in $\text{cm} \cdot \text{yr}^{-1}$ (Fig. 4b).

6.1.3. Sedimentation rate and carbon burial

Not all carbon that settles on the bottom is mineralized, but a certain fraction is (permanently) buried, at least at the timescales we consider. Several authors have demonstrated that the relative amount of carbon that is permanently buried is closely and positively related to the sedimentation rate (Henrichs and Reeburgh, 1987; Canfield, 1993; Middelburg et al., 1993). In the model we call this buried carbon “refractory.” Because the anoxic mineralization processes are not limited by the oxidants (they are not modeled), permanent burial cannot be modeled by exhaustion of all available oxidants. Hence, there is a need to incorporate this process as such.

The flux of refractory carbon is given by the equation ($r^2 = 0.93$, $N = 102$)

$$\text{Flux}C_{\text{ref}} = 1.9w^{1.31},$$

where w is in $\text{cm} \cdot \text{y}^{-1}$ and $\text{Flux}C_{\text{ref}}$ is in $\text{mM} \cdot \text{cm}^{-2} \cdot \text{y}^{-1}$ (Fig. 4c).

It should be noted that the significance of this regression stems from the fact that the sedimentation rate is used for calculating carbon burial.

From this organic burial, the concentration of refractory carbon in the sediment, under constant flux conditions can be calculated as

$$C_{\infty} = \frac{\text{Flux}C_{\text{ref}}}{w_{\infty}(1 - \Phi_{\infty})}.$$

Using the values from the model, the carbon weight content in the lower part of the modeled sediment column varies from 0.5% at a sedimentation rate of $0.001 \text{ cm} \cdot \text{y}^{-1}$ to about 2% at a sedimentation rate of $0.1 \text{ cm} \cdot \text{y}^{-1}$.

6.1.4. Water depth and temperature

Temperature has an effect on the degradability of the organic matter and on the value of the molecular diffusion coefficient.

In the model temperature changes from 15°C in the surficial layers of the water column to about 4°C at depths greater than 2000 m according to a sigmoidal function given by

$$\text{Temp}_{\text{Depth}} = T_{\infty} + (T_0 - T_{\infty}) * \left(1 - \frac{\text{Depth}^s}{\text{Depth}^s + K_D^s}\right),$$

where T_{∞} and T_0 are the temperature at infinite depth and at the surface respectively (set as 4 and 15°C , respectively), K_D is the inflection point, i.e., the depth where the temperature is

Table 8. Literature data used in the various regressions. Indicated is the number of data points.

- (1) = Sedimentation rate vs water depth
 (2) = Carbon mineralized vs sedimentation rate
 (3) = Carbon buried vs sedimentation rate
 (4) = Solid deposition vs sedimentation rate
 (5) = Irrigation enhancement factor
 (6) = Oxidic mineralization vs total mineralization
 (7) = Denitrification vs total mineralization
 (8) = Anoxic mineralization / sulfate reduction vs total mineralization
 (9) = Ammonium fluxes vs total mineralization
 (') = Only those with less than 1 cm core loss
 (**) = O₂, NO₃ and Si flux pooled
 (*** = Excluding the value from the deepest station
 (****) = Assuming all denitrification is linked to carbon mineralization
 (***** = excluding DSDP stations and data obtained from other sources

Reference	Area	(1)	(2)	(3)	(4)	(5)	(6)	(7)	(8)	(9)
ARCHER and DEVOL (1992)	Washington shelf & slope	-	-	-	-	7(***)	-	-	-	-
BAKKER and HELDER (1993)	Skaggerak, NE North Sea	21	21	22	-	-	-	-	-	-
BENDER and HEGGIE (1984)	E Pacific/E. Atlantic	4	4	4	-	-	5	5	5	-
BERELSON et al. (1987)	California borderland	-	-	-	-	-	-	-	-	2
BERNER and WESTRICH (1985)	Long Island Sound	-	-	-	4	-	-	-	-	-
CANFIELD (1988) (****)	Various	3	3	-	5	-	3	3	2	-
CHANTON et al. (1987)	Various	-	-	-	4	-	-	-	-	-
DEVOL & CHRISTENSEN (1993)	N.E. Pacific	-	-	-	-	34(***)	8	8(****)	8	8
HEGGIE et al. (1987)	Bermuda, Hatteras	11	7(**)	-	-	-	10	10	10	-
HELDER (1989)	Indian Ocean, Savu Basin	2	2	-	-	-	2	2	2	2
JØRGENSEN (1977)	Danish Coast Limfjorden	-	-	-	-	-	-	-	1	-
JØRGENSEN et al. (1990)	Baltic-North Sea transition	7	6	6	6	-	-	-	6	-
JAHNKE (1990)	California borderland	-	-	4	-	-	2	-	-	-
MARTIN et al. (1991)	Central East Pacific	5	-	-	-	-	-	-	-	-
REIMERS and SUSS (1983)	Peru continental margin	2	2	2	-	-	-	-	-	-
REIMERS et al. (1992)	Central East Pacific margin	7	7	7	-	-	8	8	8	-
RODEN and TUTTLE (1993)	Chesapeake Bay	-	-	-	3	-	-	-	-	-
SARNTHEIM et al. (1988)	Various	57	-	57	-	-	-	-	-	-

exactly inbetween T_z and T_0 (set as 500 m), and S is a shape factor denoting the steepness of the gradient (set as 2). The temperature in the sediment is assumed to be the same as in the overlying water column.

6.1.5. Water depth and reactivity of the organic matter

The organic particles settling on the sea bottom have a different composition than those in the surface water, because of decomposition in the water column. As they need more time to reach the sediment at greater depths, their mean reactivity will likely be lower there.

The reactivity of the organic matter settling on the bottom is modeled assuming that all organic matter is derived from the surface water mass and has originally the same composition. We furthermore assume that only the faster settling particles reach the sediment. The metabolizable organic matter in the upper water column consists for a fraction p_f of fast decaying matter with first-order decay constant r_f , and a fraction $(1 - p_f)$ of slowly decaying carbon with decay constant r_s . We assume that the mean sedimentation rate of settling matter equals $100 \text{ m} \cdot \text{d}^{-1}$ (Lampitt, 1985) and that there is no lateral transport. While sinking, the concentrations of both degradable fractions decrease. Also the temperature changes with depth, which affects the degradation rates of both fractions (with a Q10 value of 2). The water column is divided in layers of 10 m thickness, and both the decreasing concentration and the changing degradabilities are monitored while both organic fractions sink to the bottom. For the initial rate constants r_f and r_s (defined at a temperature of 20°C) and p_f , the fraction of fast-decaying detritus, we take the coefficients from the experiments of Westrich and Berner (1984) as derived by Boudreau and Ruddick (1991): $p_f = 0.74$, $r_f = .07 \text{ d}^{-1}$ (26 y^{-1}), $r_s = .0007 \text{ d}^{-1}$ (0.26 y^{-1}).

6.1.6. Sedimentation rate and bioturbation coefficient

According to Boudreau (1994) the intensity of mixing is related to the sedimentation rate according to a power law. Although some caution should be exercised because of the large variability, the equation proposed by Boudreau (1994) was used (after modification to daily rates):

$$D_b = \frac{15w^{0.6}}{365},$$

where D_b is in $\text{cm}^2 \cdot \text{d}^{-1}$ and w is in $\text{cm} \cdot \text{y}^{-1}$.

6.1.7. Sedimentation rate and the fraction of ODU that is permanently lost as solids

During the reduction of sulphate, part of the sulfide is buried as pyrite and cannot be reoxidized in the absence of bioturbation (Berner, 1970). The relationship between the fraction of total reduced sulfur production that is permanently deposited as solids (f_s) vs. sedimentation rate is given by ($r^2 = 0.48$; $N = 22$):

$$f_s = 0.233w^{0.336},$$

where w is in $\text{cm} \cdot \text{y}^{-1}$ (Fig. 4d). As sulfate is the most abundant electron acceptor used in the anoxic degradation process, and correcting for stoichiometry, we set half this value equal to the amount of ODU that are inaccessible to subsequent oxidation in the oxidized layer.

6.1.8. Water depth and biological irrigation

In shallow sediments, biota may enhance the flux of solutes across the bottomwater interface (Aller, 1984; Christensen et al., 1984; Archer and Devol, 1992; Devol and Christensen, 1993). By increasing the sediment uptake of

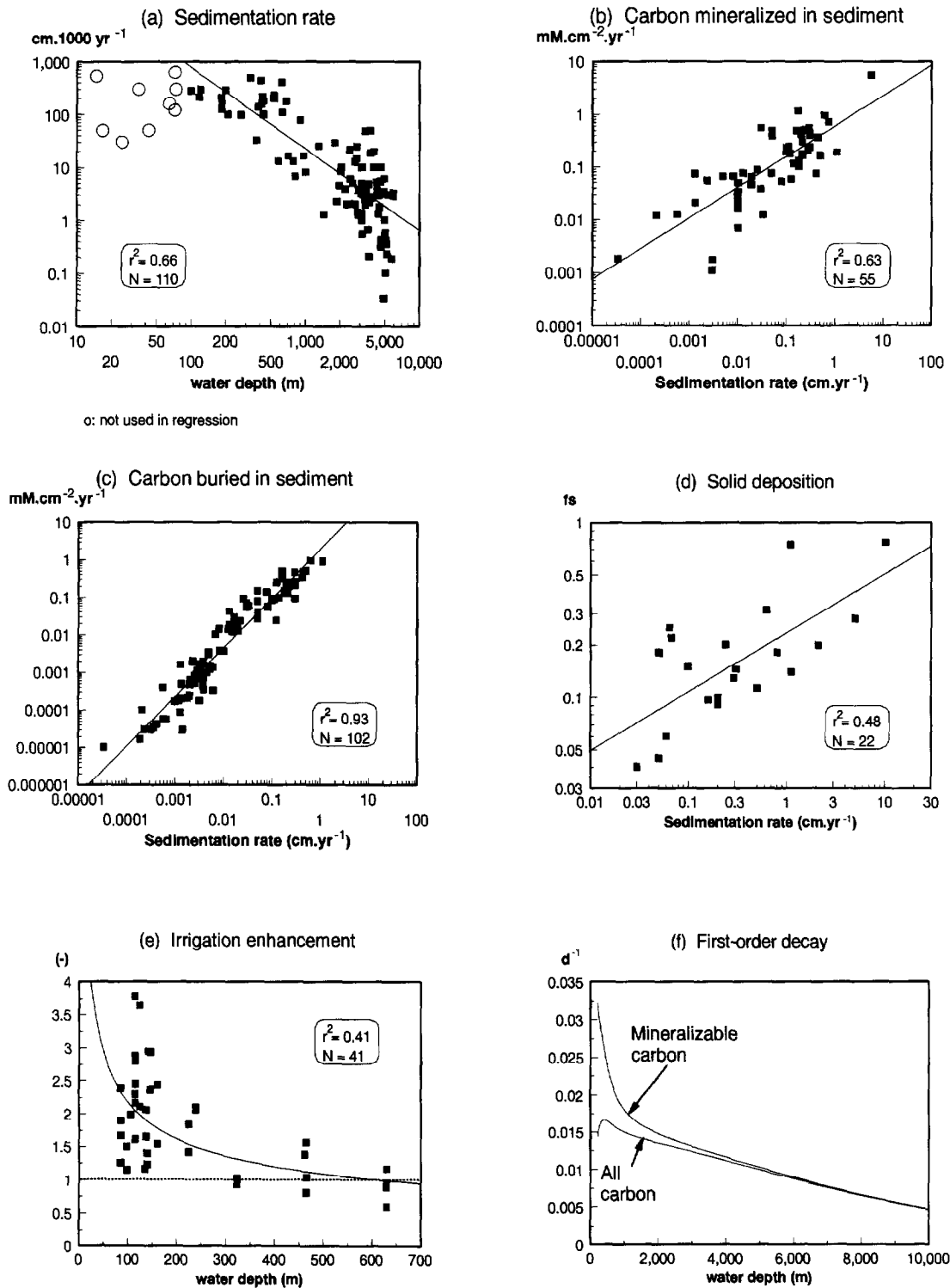


Fig. 4. Relationships between several variables used for calibrating the model; data of (a)–(e) are from the literature (for a list of references see Table 8). Figure 4f gives the first-order degradation rates of total (mineralizable + refractory) and mineralizable carbon at the bottomwater interface versus water depth used in the model.

oxygen and/or nitrate, this biologically mediated irrigation may significantly alter the relative importance of oxic and anoxic mineralization. There are several ways to incorporate this into a diagenetic model, either as an enhanced diffusive

flux or as nonlocal exchange. On theoretical grounds, the latter model is to be preferred, because it is consistent with more complex radial-diffusion models of irrigation (Aller, 1980; Boudreau, 1984). The most pragmatic treatment of

mixing is by means of a diffusion enhancement factor, which, multiplied with the sediment diffusion coefficient gives the apparent "bio-diffusion" coefficient. As this diffusion enhancement factor is very near to the ratio of the measured flux to the flux due to molecular diffusion, it can be readily estimated from literature data. This was the approach adopted in our model. Furthermore, we assumed that the enhancement factor had the same profile as the bioturbation coefficient, i.e., maximal in the constant bioturbation layer, and decreasing to nonenhancement (factor = 1) below this layer.

The diffusion enhancement factor was obtained by regression of values in Devol and Christensen (1993) and of Archer and Devol (1992, excluding the deepest value) against depth ($r^2 = 0.41$, $N = 41$; Fig. 4e):

$$\text{IrrEnh} = \text{MIN}(1, 15.9D^{-0.43});$$

in the model this factor was not allowed to be lower than 1. In the bioturbation layer, then

$$D_{\text{sed},x} = \text{IrrEnh} * D_s^T$$

is the sediment diffusion coefficient used instead of D_s^T , while below this constant bioturbation layer,

$$D_{\text{sed},x} = \text{IrrEnh} * D_s^T * e^{[-(x-xb)/\text{coeff}Db]}$$

is used.

7. MODEL RESULTS AND DISCUSSION

7.1. Distribution Along a Mineralization Gradient

The ability of the model to reproduce observed rates was tested by means of two runs, one with well-oxygenated bottomwater and low nitrate concentration (oxygen concentration of $200 \mu\text{mol} \cdot \text{L}^{-1}$, nitrate = $20 \mu\text{mol} \cdot \text{L}^{-1}$), and another with low oxygen and high nitrate bottomwater concentration (20, respectively, $40 \mu\text{mol} \cdot \text{L}^{-1}$). The literature data used to calibrate the model (Table 8) are represented as functions of total flux of mineralizable carbon, as this gives the least scatter (Fig. 5). Best parameter values are listed in Table 6. The general trends in oxic mineralization, denitrification, and anoxic mineralization are reasonably well represented, considering the large amount of simplifying assumptions. When carbon flux is low, oxygen is the major electron acceptor, even when its concentration in the bottomwater is low. Increasing the total flux of mineralizable carbon results in a decreased fraction of carbon mineralized by oxygen, while the other pathways gain in importance. The relative contribution of the denitrification process shows no straightforward relationship with increasing flux and depends mainly on the concentrations of oxygen and nitrate in the overlying bottom water (see below).

7.2. Sediment-Depth Profiles

The modeled profiles of oxygen, nitrate, and carbon for the stations at 200, 1000, and 3000 m under the two contrasting bottomwater concentrations are illustrated in Fig. 6.

When the concentration of oxygen in the water column is low, oxygen is depleted a few millimeters under the sediment-water interface (all stations), while beneath the well-

aerated water column, oxygen penetrates about 1 cm (200 m depth), 2 cm deep (1000 m), or the sediment column is fully oxic (3000 m deep).

Nitrate is produced through the oxidation of ammonium (nitrification) and is consumed by the denitrification process. The shape of the nitrate profile reflects whether the sediment actually takes up nitrate (in case where the concentration declines with sediment depth) or whether sediments act as a source of nitrate to the water column (in case where concentrations are greater below the interface than in the bottomwater). In the well-oxygenated case ($\text{BW O}_2 = 200 \mu\text{mol} \cdot \text{L}^{-1}$, $\text{BW NO}_3 = 20 \mu\text{mol} \cdot \text{L}^{-1}$), nitrification in the upper sediment layer proceeds fast enough to build up higher concentrations in the upper sediment layers; hence, nitrate diffuses into the overlying water column. The depth of the nitrate peak and the total nitrate standing stock increase with increasing water depth, indicating that denitrification proceeds deeper down into the sediment. At 3000 m depth, denitrification does not produce a visible reduction in nitrate concentration (the process contributes for less than 1% of total mineralization). In the low oxygen condition ($\text{BW O}_2 = 20 \mu\text{mol} \cdot \text{L}^{-1}$, $\text{BW NO}_3 = 40 \mu\text{mol} \cdot \text{L}^{-1}$), the denitrification consumes all nitrate in the upper 2 cm (200 m depth) and in the upper 4 cm (1000 m depth), while at 3000 m depth nitrate is substantially decreased in the deeper sediment layers, but it is not entirely exhausted (Fig. 6).

Because carbon mineralization is not limited by total oxidant concentration, TOC profiles for both contrasting bottomwater conditions are the same. In the absence of bioturbation, carbon concentrations decline according to their reactivity (the more reactive, the faster carbon concentrations decrease, the stronger the spatial gradient) and the sediment burial rate (at higher burial rates, carbon is much younger and hence less degraded at comparable depths, resulting in a reduced gradient). Bioturbational mixing tends to smoothen the carbon gradient. These processes can be seen at work in the profiles of mineralizable carbon (Fig. 6): concentrations decline more or less continuously till a depth of 5 cm (which marks the lower limit of the constant bioturbation layer see Fig. 3). As bioturbation decreases rapidly beyond this layer, the gradient becomes more pronounced until all mineralizable carbon has been consumed. Notice that, in the model, the mean reactivity of carbon also declines with sediment depth, which affects the curvature of the carbon profile. Because bioturbative mixing, as well as sediment burial, are lowest in the deepest station, carbon concentrations decline most rapidly here, and the penetration depth of mineralizable carbon increases from the deepest towards the shallowest station. The somewhat lower reactivity of carbon at highest water depth (which tends to increase carbon penetration) is relatively unimportant compared to bioturbation and sedimentation effects.

7.3. Sensitivity Analysis

The influence of several factors on the relative importance of the different mineralization pathways was investigated by varying the input of mineralizable carbon, the oxygen, and the nitrate concentration in the bottomwater, the bioturbation coefficient, the sedimentation rate, and the reactivity of the

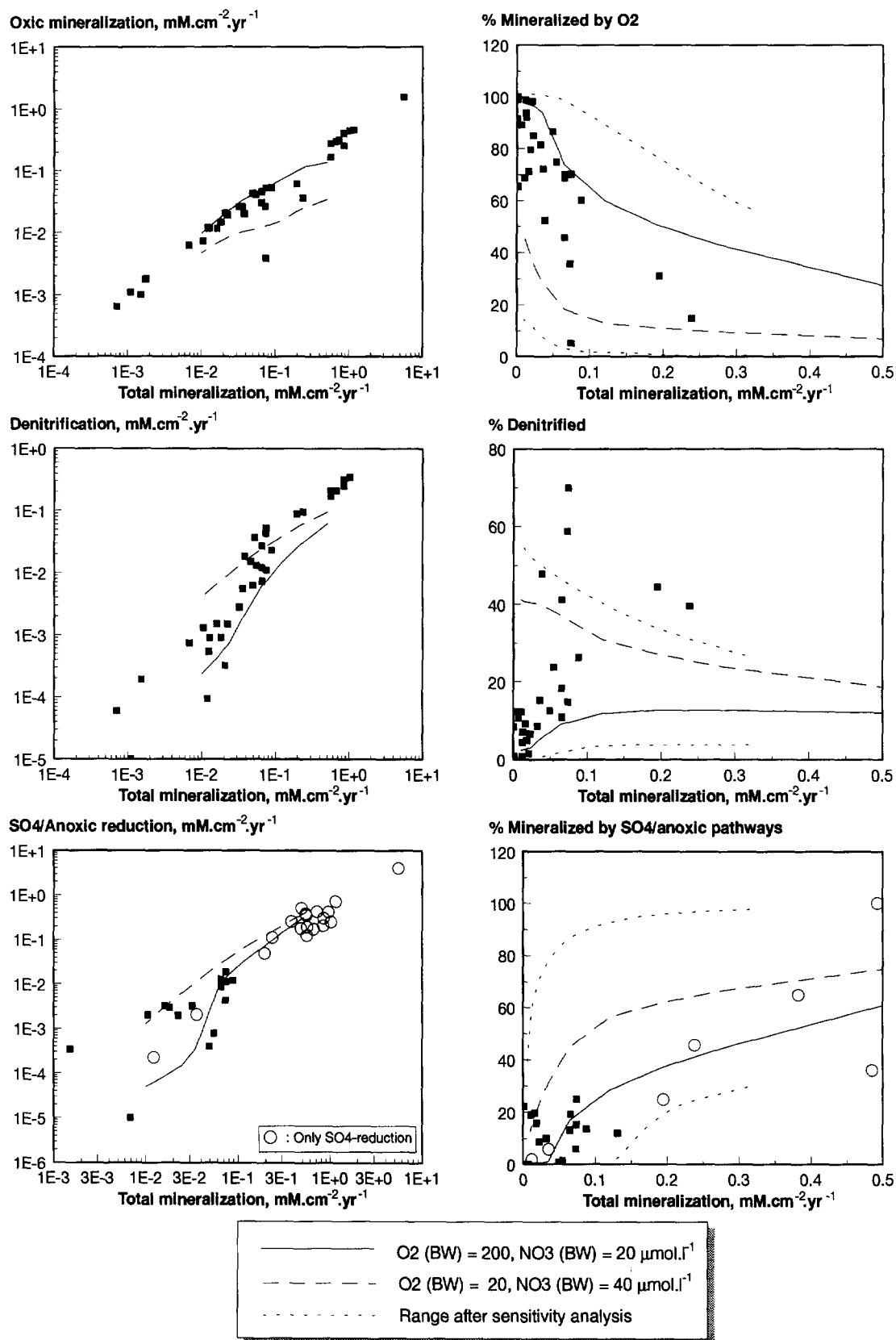


Fig. 5. A comparison of two model runs with different bottomwater concentrations of oxygen and nitrate with literature data (for a list of references see Table 8). Indicated in dashed lines is the range obtained after sensitivity analysis (see results and discussion).

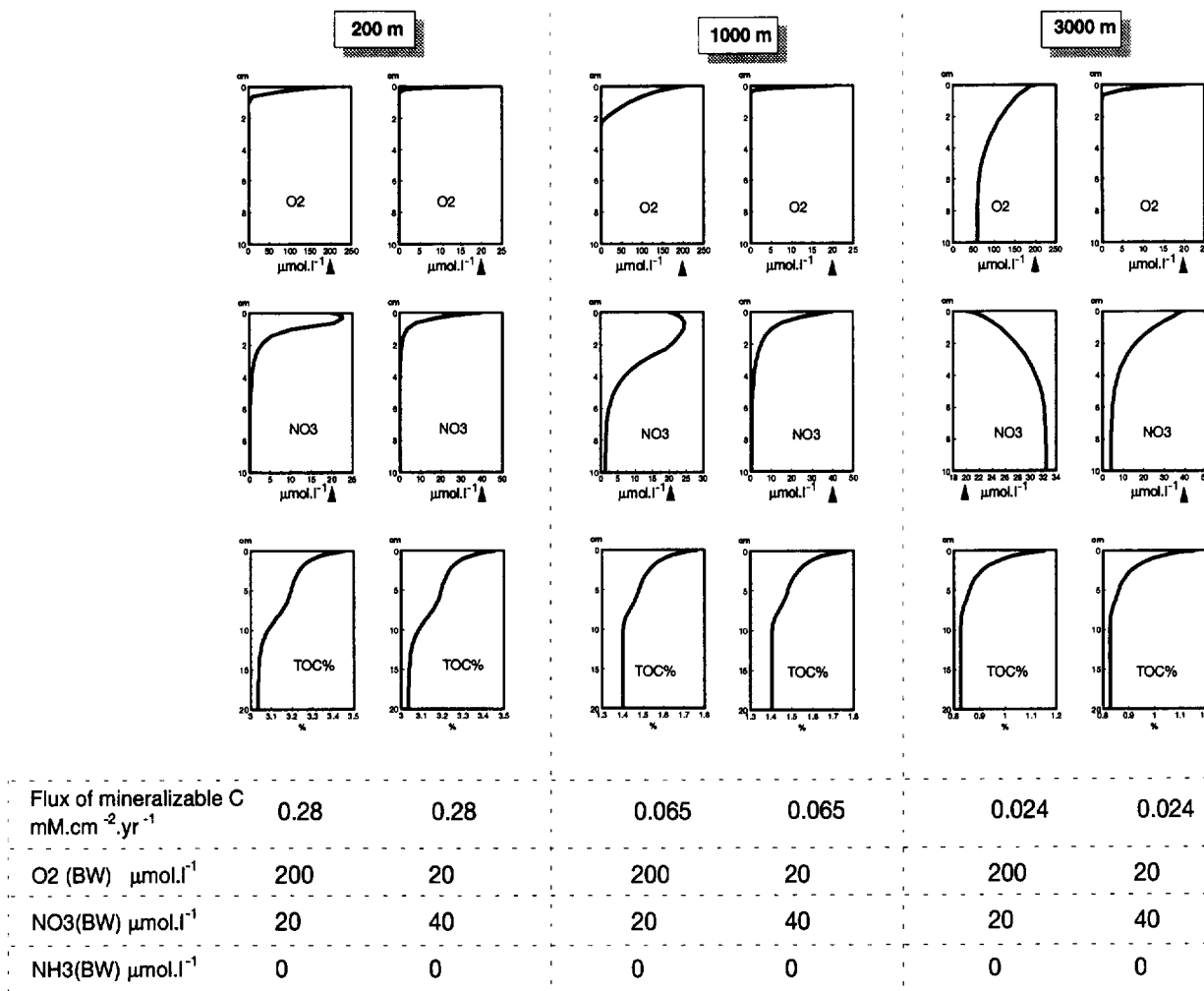


Fig. 6. Model oxygen, nitrate, and carbon profiles at 200, 1000, and 3000 m depth under high-oxygenated (left) and low oxygenated (right) bottomwater. Indicated with the arrow is the bottomwater concentration.

organic matter. Three thousand sets of parameter values were randomly drawn within a specified interval using a uniform latin hypercube subsampling procedure and the steady-state condition of each set was calculated. We used the mean parameter set of the station at 1000 m depth as a starting point. The sedimentation rate and the bioturbation coefficient were allowed to vary within two orders of magnitude (i.e., the minimum value = mean rate/10, maximum = mean rate · 10). The flux of mineralizable carbon and reactivity were at least one-fifth of the mean rate and at most five times the mean rate; oxygen bottomwater concentrations were varied between 10 and 300 $\mu\text{mol} \cdot \text{L}^{-1}$, nitrate bottomwater concentrations were varied between 5 and 50 $\mu\text{mol} \cdot \text{L}^{-1}$. The total ranges used in the sensitivity analysis, the percentage contribution of each mineralization pathway at the minimal and maximal value of each factor, and the correlation between the different mineralization pathways and these variables are given in Table 9a, b, and c. Total oxic mineralization varied from 1 to 98%, denitrification varied from 1 to 54%, while anoxic mineralization varied from 0 to 95% of total mineralization. The total range of

values is also given in Fig. 5. Note that the high values of denitrification reported in Reimers et al. (1992) cannot be reproduced.

The concentrations in the overlying water column directly affect the amount of substance that can be drawn into the sediment (Fig. 6); hence, the oxygen concentration of the water column favors the oxic pathway, while the denitrification and the anoxic pathway are negatively influenced (Table 9c). Increasing the nitrate concentration favors the denitrification when compared to anoxic mineralization. The small positive effect of increased nitrate concentration on oxic mineralization is probably due to the lowered production of oxygen demand units resulting from the suppression of anoxic processes.

Besides lowering the oxygen concentration, the importance of the oxic mineralization pathway is most significantly depressed by increasing the total carbon flux or bioturbative mixing; the former because a higher demand of oxidantia near the surface (Fig. 7c) causes steeper gradients of oxygen whereas the general shape of carbon consumption remains unaffected (compare Fig. 7a with 7c or 7b with 7g), the

Table 9. Results of the sensitivity analysis involving the oxygen and nitrate concentration in the overlying water (O2BW, resp. NO3BW), sedimentation rate (sedrate), the bioturbation coefficient (Db), the flux of mineralizable matter (Minflux) and the mean reactivity of sedimenting organic carbon (React). Oxic = oxic carbon mineralization; denit = denitrification; Anoxic = carbon mineralization in the anoxic pathway.

A. The total range used in the calibration

Range	O2BW $\mu\text{mol.l}^{-1}$	NO3BW $\mu\text{mol.l}^{-1}$	Sedrate cm.kyr^{-1}	Db $\text{cm}^2.\text{yr}^{-1}$	Minflux $\mu\text{M.cm}^2.\text{y}^{-1}$	React yr^{-1}	%Oxic %	%Denit %	%Anoxic %
Mean	154.5	27.0	112.5	7.7	169	16	30.0	13.5	56.5
Max	300.0	50.0	222.9	15.3	325	30	98.4	54.1	94.6
Min	10.0	5.0	2.2	0.15	13	1	1.4	0.9	0.2

B. The % contribution of the different pathways at the minimal and maximal value of each factor (keeping the other factors at their calibration value)

Values	Calibration run 1000m	O2BW 10	NO3BW 300	Sedrate 5	Db 50	Minflux 2.2	React 222.9	Db 0.0004	Minflux 0.013	React 0.003
%Oxic	74	11	86	73	75	75	69	96	38	97
%Denitr	9	25	7	6	13	9	9	3	14	2
%Anoxic	17	65	7	20	12	16	22	1	48	1

C. Correlation of the factors with the different mineralization pathways

corr. coeff	O2BW	NO3BW	Sedrate	Db	Minflux	React	%Oxic	%Denit	%Anoxic
%Oxic	0.51	0.01	-0.00	-0.34	-0.61	0.03	1		
%Denitr	-0.32	0.66	-0.00	0.00	-0.20	-0.04	-0.23	1	
%Anox	-0.45	-0.17	0.00	0.35	0.68	-0.02	-0.97	-0.01	1

latter because it transports carbon away towards deeper layers (Fig. 7i). Increasing the reactivity of the organic matter causes it to degrade more towards the surface (Fig. 7h), increasing the oxygen demand (Fig. 7d) and the contribution of the oxic pathway in total mineralization, but this effect is negligible compared to the effects of total carbon flux, oxygen concentration and bioturbation (Table 9c). Similarly, the sedimentation rate has only a small effect on the mineralization pathways (Table 9c). The fact that bioturbation has a large influence while the sedimentation rate only marginally affects mineralization processes is due to their different impact on both degradable fractions. Whereas the sedimentation process affects both degradable fractions equally, increasing the bioturbation has a greater effect on the fast decaying carbon compared to the slowly decaying fraction (the gradients are much more pronounced in the former). The difference in carbon penetration which is caused by changing the sedimentation rate (Fig. 7j) can be ascribed mainly to the slowly degradable fraction; hence, it is not translated in large differences in carbon consumption rates (Fig. 7f). On the contrary, the effect of bioturbation on carbon consumption rates is high (because of its strong influence on the distribution of fast detritus, Fig. 7e), which explains why this parameter has such a large effect on the oxic mineralization (Table 9c).

When carbon escapes the zone of oxic degradation, the denitrification benefits first up till a depth where carbon is shunted below the nitrate zone, after which anoxic processes take over. This explains why, on the average, denitrification is less affected (or seemingly unaffected) by changes in reactivity, bioturbation, and total mineralization flux (Table 9c).

The shape of the porosity profile was shown to have important consequences on the penetration depth of oxygen in the sediment (Rabouille and Gaillard, 1991a), but these authors did not include the effect of porosity on the

bulk sediment diffusion coefficient. Although we did not include the shape of the porosity profile in the sensitivity analysis, its effect was examined with two runs, one with a very strong curvature in porosity (coefficient of 1); the other run with a gentle porosity decline (coefficient = 10). Increasing the curvature (and hence decreasing mean porosity at a certain depth) lowered the relative contribution of oxic processes by at most one third (at the highest flux stations). This is due to the smaller value of the bulk sediment diffusion coefficient at lower porosities, which lowers the flux of oxygen into the sediment. Denitrification was not uniformly affected by the changing porosity profile: the greatest change was 20%. Note also that Rabouille and Gaillard (1991a) demonstrated the opposite effect, an increase of the oxic mineralization pathway with decreasing porosity.

In the model the oxygen demand units were given a dispersion coefficient equal to HS^- , as this is the product of the most prominent anoxic mineralization process in the marine environment (sulphate reduction). However, in intermediate sedimentary regimes, manganese and iron oxide reduction may be more important than sulphate reduction. As anions (e.g., HS^-) diffuse faster than cations (e.g., Mn^{++} ; Li and Gregory, 1974), the value of the diffusion coefficient of ODU was overestimated in these cases. We examined the effect of this at three intermediate stations (500, 1000, and 2000 m depth), for two contrasting bottomwater cases, using the diffusivity of Mn^{++} . Because the ODU now diffuse much slower (about a factor 3), less escapes to the overlying bottomwater and more is oxidized in the sediment column itself. As there is thus less oxygen available for oxidizing carbon, the oxic mineralization pathway is negatively influenced, to the benefit of both the denitrification and the anoxic mineralization process. The difference is most pronounced in the shallowest station (500 m), where the relative contribution of the oxic mineralization drops from 60 to 58%

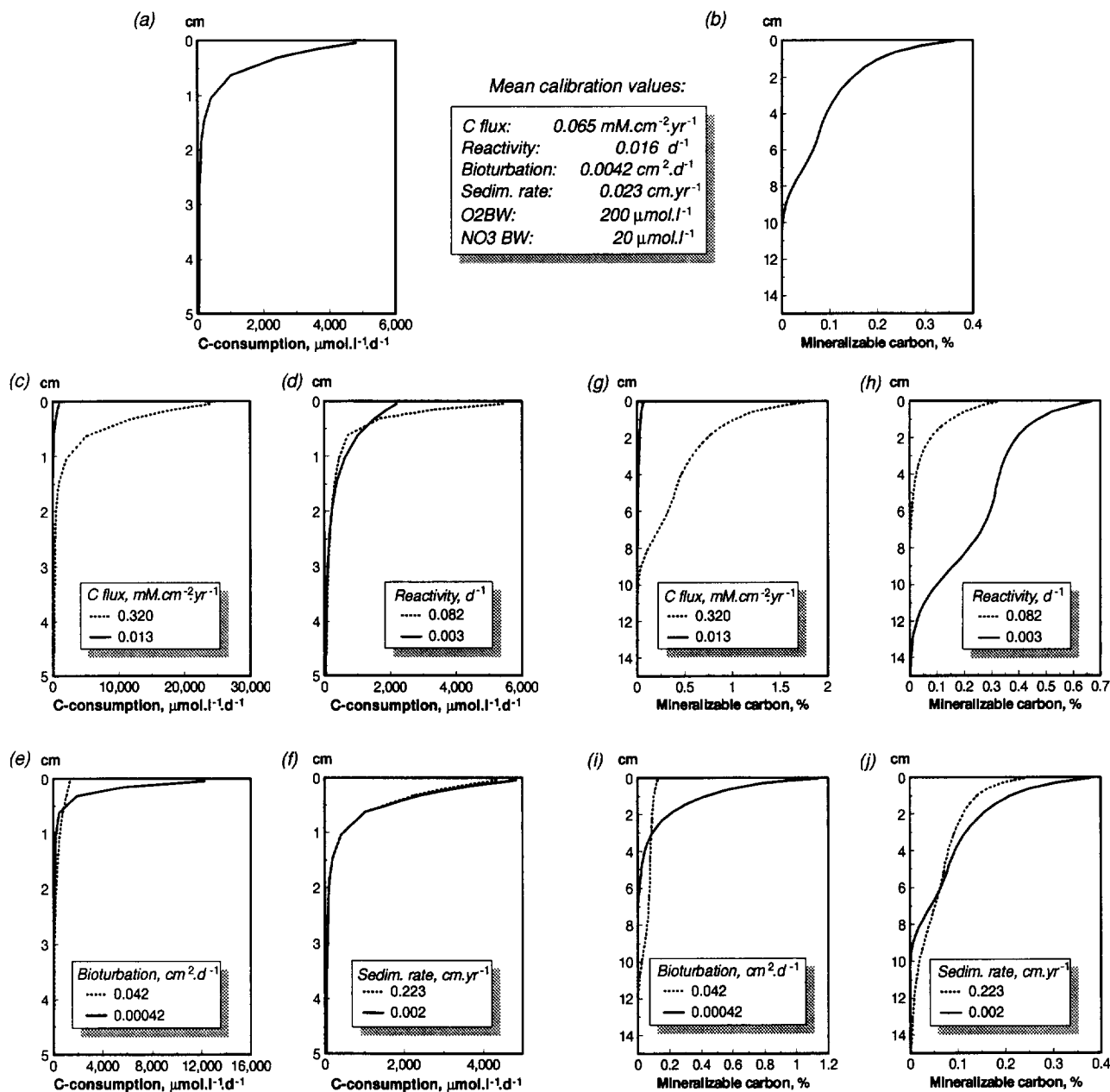


Fig. 7. The impact of varying the carbon flux (c, g), reactivity (d, h), bioturbation (e, i), and sedimentation rate (f, j) on sediment profiles of mineralizable carbon (i.e., fast-decay + slow-decay carbon) (right) and on total carbon consumption rates (left). Above (a, b) are the profiles using the mean parameter values. The relative contribution of the different mineralization pathways, corresponding with this figure are in Table 9c.

under well-aerated bottomwater, from 13 to 10% under a poorly aerated water column.

7.4. Fine-Scale Distribution of Oxygen-Demand Processes

The fine-scale distribution of oxygen-demand processes in our model is represented in Fig. 8, for the case of well-oxygenated bottomwater. Oxygen is consumed by carbon oxidation, by nitrification, and by oxidation of reduced substances (ODU). At 3000 m depth, anoxic processes contrib-

ute only marginally to total mineralization and the oxygen demand resulting from ODU oxidation is negligible. Oxygen in this station is consumed by the (oxic) mineralization process (76%) and by the subsequent oxidation of the generated ammonium (22%). As both depend on the carbon concentration and reactivity, which decrease with depth into the sediment, total oxygen demand continuously decreases with sediment depth (Fig. 8c). As a result, the oxygen profile has a gent curvature, which resembles the shape of the nitrate profiles of Fig. 6. (Nitrate too is only consumed by carbon mineralization in the model.)

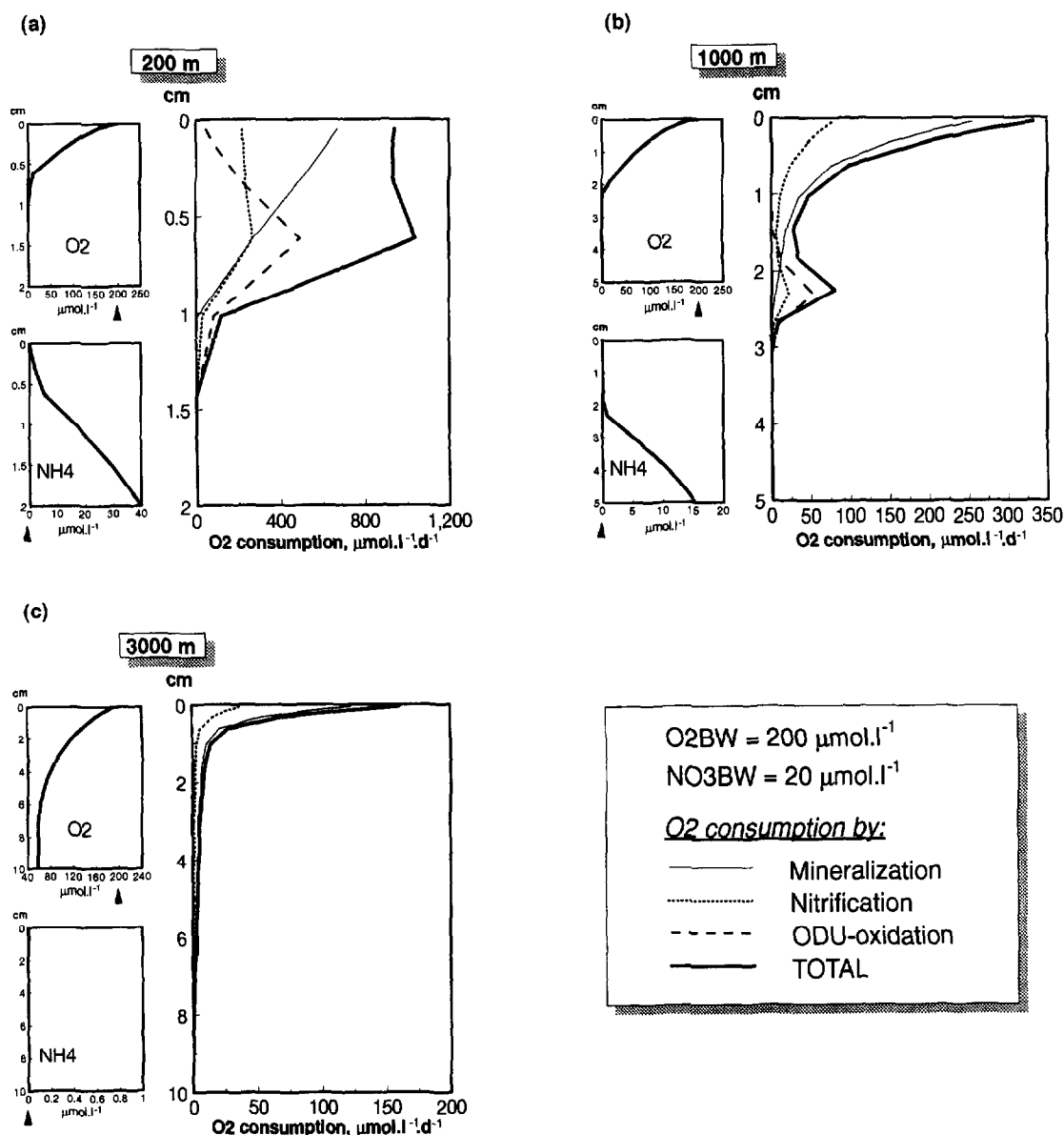


Fig. 8. Modeled distribution of oxygen demanding processes (large) and oxygen and ammonium profiles (small) for the stations at 200, 1000, and 3000 m depth.

At shallower depths, anoxic mineralization is important. At 200 m depth, the oxic mineralization consumes 41% of all the oxygen, the nitrification consumes another 25%, while 34% is due to ODU oxidation; at intermediate depth (1000 m) the figures are 62, 24, and 14% respectively. Anoxic processes occur deeper down in the sediment where oxygen is depleted and the reduced substances formed (in the model ammonium and ODU) diffuse upward. As the oxygen concentration increases, they are oxidized quickly. This provokes an oxygen demand which can be spatially separated from the one linked to the oxic mineralization: it peaks at the depth that has the best mix of reduced substances and oxygen concentration, i.e., the base of the oxic zone. At the shallowest station (200 m), oxygen penetration is small, the spatial separation of the oxygen demanding processes is not very strong and total oxygen demand is more or less constant

in the upper centimeters. After this it drops to much lower levels (Fig. 8a). As a consequence, the oxygen concentration decreases almost linearly in the upper centimeter. At intermediate depth (1000 m), the spatial separation of processes linked to oxic mineralization (and consecutive nitrification) and of oxidation of deeper-formed reduced substances is most pronounced and total oxygen demand is bimodal (Fig. 8b). A similar bimodal consumption of sulphate, caused by carbon oxidation (surficial peak) and methane oxidation (deeper peak) was described amongst others by Iversen and Jørgensen (1985).

The literature frequently describes oxygen consumption processes in the sediment either as a 0-th order consumption term, i.e., a depth-independent O₂ uptake rate per unit volume (Bouldin, 1967; Revsbeck et al., 1980; Helder, 1989) or as an uptake which is first-order to carbon concentration

(Archer and Devol, 1992; Murray and Kuivila, 1990; Emerson et al., 1985). The use of 0-th order uptake has been justified by the assumption that carbon is not limiting and because of the relative insensitivity of most microbial oxygen-demanding processes for O_2 , when its concentration is higher than about $10 \mu M$ (Helder, 1989). Our model indicates that in shallow areas O_2 consumption may indeed be of apparent 0-th order, not because of the reason mentioned above, but because of the proximity of the sites of oxic mineralization and reoxidation processes in the sediment. In the deeper regions however, oxygen demand is proportional to carbon degradability.

7.5. Reactivity of the Organic Matter

One of the least understood factors in our model is the reactivity of the organic matter at the time it becomes incorporated into the sediment. We tried to estimate this reactivity by modeling the settlement of organic matter through the water column, assuming that the original pool (in the upper layer of the water column) was the same at all stations, that settling occurred at a fixed rate ($100 m \cdot d^{-1}$) and that there was no lateral excursion or resuspension. Reality is somewhat more complex. A large range of sinking speeds have been reported in the literature (from a few $m \cdot d^{-1}$ to a mean of $100\text{--}150 m \cdot d^{-1}$ in Billett et al., 1983; up to $3200 m \cdot d^{-1}$ for pellets in Honjo et al., 1982). Particles that sink faster will contribute relatively more to what settles on the bottom. Currents can resuspend phytodetritus when speeds are above $7 cm \cdot s^{-1}$ (Lampitt, 1985), a value which is not unusual for sites along ocean margins. These resuspension events will augment the residence time of the particles in the water column, during which carbon reactivity will further decrease (Walsh, 1992).

Despite the simplifying assumptions on which our reactivity estimates are based, they are consistent with data reported in the literature. Mean degradability at the bottomwater interface in the model (including the refractory part) changes from $.035 d^{-1}$ ($13 y^{-1}$) at 300 m depth to $.007 d^{-1}$ ($3 y^{-1}$) at 8000 m depth; it is $.011 d^{-1}$ ($4 y^{-1}$) at 4500 m (Fig. 4f). Lochte and Turley (1988) reported degradation rates of $.018 d^{-1}$ ($7 y^{-1}$) for phytodetritus deposited directly after the spring bloom, at 4500 m depth in the North Atlantic. In order to reproduce observed responses of benthic oxygen demand to seasonally varying fluxes of POC (Smith et al., 1992), Sayles et al. (1994) showed that the first-order mineralization constant of sedimenting matter in a northeast Pacific site at 4000 m depth should be at least 5 to $10 y^{-1}$ ($0.01\text{--}0.03 d^{-1}$), similar to our model values; on the other hand, they argued that rate constants at an oligotrophic site near Bermuda (4400 m) were much less than $1 y^{-1}$ ($0.003 d^{-1}$). While the latter data are not consistent with our simple approach, this does not cause a major problem as the sensitivity analysis showed that the effect of varying the degradability on the outcome of the model is rather limited (Table 9).

The one to two order-of-magnitude difference between first-order decay of particles in the water column (Westrich and Berner, 1984) and in the sediments (e.g., Jahnke, 1990) is often used as an indication of extensive diagenesis during

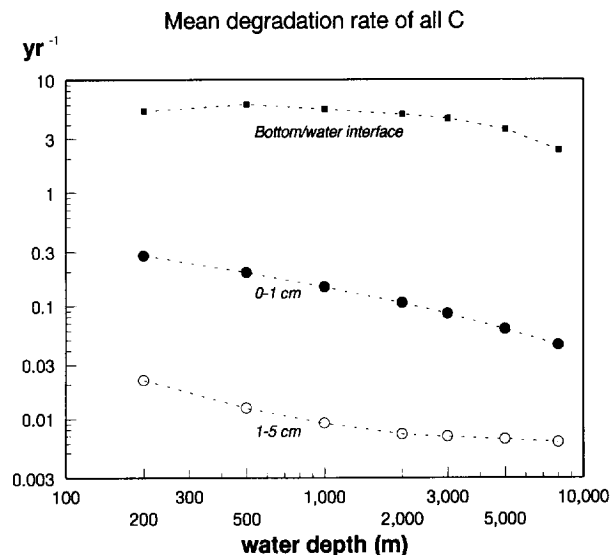


Fig. 9. A comparison of the mean first-order degradation constant (y^{-1}) of all carbon (mineralizable + refractory) at the sediment-water interface, in the upper centimeters and in the 1–5 cm sediment layer.

the rebound process (Walsh, 1992). In Fig. 9, we have compared the mean degradation rate of total organic carbon (mineralizable + refractory) at the sediment-water interface with organic carbon in the upper centimeter and in the 1–5 cm sediment layer. There is one order of magnitude difference between the interfacial degradability ($2\text{--}6 y^{-1}$) and the mean degradability in the upper centimeter ($0.05\text{--}0.3 y^{-1}$). The carbon in the deeper layers (1–5 cm) has a mean reactivity which is another order of magnitude lower ($0.007\text{--}0.02 y^{-1}$). The mean residence time of carbon in the model (with respect to degradation) varies then from 3 to 20 years in the upper centimeter and from 40 to 140 years in the 1–5 cm layer. These values are within ranges reported from sediments along the ocean margin ($1\text{--}680 y$ in Emerson and Hedges, 1988). Similarly, Martin et al. (1991) calculated that the average lifetime of organic carbon in the upper centimeter varied from three years at high flux stations to eleven years at low flux stations (all deeper than 4000 m). Thus, although the organic matter that arrives at the sediment surface in our model is very reactive, the first-order decay rates in the sediment are comparable to published values.

8. CONCLUSIONS AND REMARKS

In this paper we have described a model of early diagenetic processes in marine sediments. The model includes oxic diagenesis, nitrification, denitrification, and anoxic processes. By lumping all anoxic processes, a great deal of uncertainties regarding internal oxidation-reduction processes (e.g., manganese oxide reaction with reduced sulfur Aller and Rude, 1988; iron oxide reaction with sulphide Canfield, 1988) are reduced, yet the impact of anoxic processes on the oxygen and nitrogen budget is approximated. We did not include nitrate consumption linked to the oxidation of reduced Manganese or iron compounds, NH_4^+ or other

reduced substances (Aller, 1990; Burdige, 1993), because these processes are not yet well understood and quantified, and they would add another (unknown) parameter to the model. Nevertheless, it could be that high values of nitrate consumption, such as those reported by Reimers et al. (1992), are related to these processes. In the model, the relatively high denitrification rates observed in certain areas are accommodated by allowing substantial overlap in the zone of nitrification and denitrification (by decreasing the inhibitory effect of oxygen on denitrification). Although this is consistent with the observation of a close coupling of the nitrification and denitrification process (Blackburn et al., 1994), it could be that the degree of inhibition of oxygen on the denitrification is allowed to be too weak in the model.

Although the model incorporates so many simplifying assumptions (concerning the reactivity of the sedimenting organic matter, no nonlocal mixing, anoxic mineralization not limited by oxidant availability, the use of 'average' forcing variables, denitrification only linked to carbon mineralization, the steady-state assumption, etc.), it is able to reproduce observed trends along sedimentary gradients and generates concentration vs. depth profiles that resemble measured ones. This reflects the objective of the model as a tool to examine the effect of nonsteady-state dynamics on profiles and fluxes along the ocean margin (Soetaert et al., 1996). It has been linked to a one-dimensional, dynamic ecological model of the water column (K. Soetaert et al., unpubl. data). This makes it possible not only to test the response of the bottom to temporarily varying properties of the water column but also the effect of this response on the water column.

Acknowledgments—The model was developed in the framework of the Ocean Margin EXchange (OMEX) project, financed by the MAST programme of the Commission of European communities (MAS2-CT93-0069). The first author acknowledges a grant as a modeler in the Biology group of the project. The final aim is to provide a global ecosystem model along the ocean margin. Dr C. Heip is thanked for critically reading the manuscript. C. Steefel, D. Burdige, D. Archer, assistant editor B. Boudreau and two anonymous reviewers are thanked for their constructive comments. This is paper number 2077 from the NIOO-CFMO. The database, collected for this research, and the model are available upon request to the authors.

Editorial handling: B. P. Boudreau

REFERENCES

- Aller R. C. (1980) Quantifying solute distributions in the bioturbated zone of marine sediments by defining an average microenvironment. *Geochim. Cosmochim. Acta* **44**, 1955–1965.
- Aller R. C. (1984) The importance of relict burrow structures and burrow irrigation in controlling sedimentary solute distributions. *Geochim. Cosmochim. Acta* **48**, 1929–1934.
- Aller R. C. (1990) Bioturbation and manganese cycling in hemipelagic sediments. *Phil. Trans. Roy. Soc. London* **331**, 51–68.
- Aller R. C. and Rude P. D. (1988) Complete oxidation of solid phase sulfides by manganese and bacteria in anoxic sediments. *Geochim. Cosmochim. Acta* **52**, 751–765.
- Archer D. and Devol A. (1992) Benthic oxygen fluxes on the Washington shelf and slope: A comparison of in situ microelectrode and chamber flux measurements. *Limnol. Oceanogr.* **37**, 614–629.
- Bakker J. F. and Helder W. (1993) Skagerrak (northeast North Sea) oxygen microprofiles and porewater chemistry in sediments. *Mar. Geol.* **111**, 299–321.
- Bender M. L. and Heggge D. T. (1984) Fate of organic carbon reaching the deep sea floor: a status report. *Geochim. Cosmochim. Acta* **48**, 977–986.
- Bender M. L., Jahnke R., Weiss R., Martin W., Heggge D. T., Orcharado J., and Sowers T. (1989) Organic carbon oxidation and benthic nitrogen and silica dynamics in San Clemente Basin, a continental borderland site. *Geochim. Cosmochim. Acta* **53**, 685–697.
- Berelson W. M., Hammond D. E., and Johnson K. S. (1987) Benthic fluxes and the cycling of biogenic silica and carbon in two southern California borderland basins. *Geochim. Cosmochim. Acta* **51**, 1345–1363.
- Berner R. A. (1970) Sedimentary pyrite formation. *Amer. J. Sci.* **268**, 1–23.
- Berner R. A. (1980a) *Early Diagenesis—A Theoretical Approach*. Princeton Univ. Press.
- Berner R. A. (1980b) A rate model for organic matter decomposition during bacterial sulfate reduction in marine sediments. In *Biogéochimie de la Matière Organique à l'interface Eau-Sédiment Marin: Colloques Internationaux du C.N.R.S. no 293*, pp. 35–44.
- Berner R. A. and Westrich J. T. (1985) Bioturbation and the early diagenesis of carbon and sulfur. *Amer. J. Sci.* **285**, 193–206.
- Billett D. S. M., Lampitt R. S., Rice A. L., and Mantoura R. F. C. (1983) Seasonal deposition of phytoplankton to the deep-sea benthos. *Nature* **302**, 520–522.
- Blackburn T. H., Blackburn N. D., Jensen K., and Risgaard-Petersen N. (1994) Simulation model of the coupling between nitrification and denitrification in a freshwater sediment. *Appl. Env. Microbiol.* **60**(9), 3089–3095.
- Boudreau B. P. (1984) On the equivalence of nonlocal and radial-diffusion models for porewater irrigation. *J. Mar. Res.* **42**, 731–735.
- Boudreau B. P. (1986) Mathematics of tracer mixing in sediments: I. Spatially-dependent, diffusive mixing. *Amer. J. Sci.* **286**, 161–198.
- Boudreau B. P. (1994) Is burial velocity a master parameter for bioturbation? *Geochim. Cosmochim. Acta* **58**, 1243–1249.
- Boudreau B. P. (1995) A method-of-lines code for carbon and nutrient diagenesis in aquatic sediments. *Computers and Geosciences* (in press).
- Boudreau B. P. and Canfield D. E. (1993) A comparison of closed- and open-system models for porewater pH and calcite-saturation state. *Geochim. Cosmochim. Acta* **57**, 317–334.
- Boudreau B. P. and Ruddick B. R. (1991) On a reactive continuum representation of organic matter diagenesis. *Amer. J. Sci.* **291**, 507–538.
- Bouldin D. R. (1967) Models for describing the diffusion of oxygen and other mobile constituents across the mud-water interface. *J. Ecol.* **56**, 77–87.
- Burdige D. J. (1991) The kinetics of organic matter mineralization in anoxic marine sediments. *J. Mar. Res.* **49**, 727–761.
- Burdige D. J. (1993) The biogeochemistry of manganese and iron reduction in marine sediments. *Earth Sci. Rev.* **35**, 249–284.
- Canfield D. E. (1988) Sulfate reduction and the diagenesis of iron in anoxic marine sediments. Ph.D. dissertation, Yale Univ.
- Canfield D. E. (1993) Organic matter oxidation in marine sediments. In *Interactions of C, N, P, and S Biogeochemical Cycles and Global Change* (ed. R. Wollast et al.), pp. 333–364. Springer-Verlag.
- Chanton J. P., Martens C. S., and Goldhaber M. B. (1987) Biogeochemical cycling in an organic-rich coastal marine basin. 7. Sulfur mass balance, oxygen uptake and sulfide retention. *Geochim. Cosmochim. Acta* **51**, 1187–1199.
- Christensen J. P., Devol A. H., and Smethie W. M. J. (1984) Biological enhancement of solute exchange between sediments and bottom water on the Washington continental shelf. *Cont. Shelf Res.* **3**(1), 9–23.
- De Hoop B. J., Herman P. M. J., Scholten H., and Soetaert K., eds. (1993) *SENECA 2.0. A Simulation Environment for Ecological Application-Manual*. Netherlands Institute of Ecology.
- Devol A. H. and Christensen J. P. (1993) Benthic fluxes and nitrogen cycling in sediments of the continental margin of the eastern North Pacific. *J. Mar. Res.* **51**, 345–372.
- Dhakar S. P. and Burdige D. J. (1996) A coupled, non-linear, steady

- state model for early diagenetic processes in pelagic sediments. *Amer. J. Sci.* (in press).
- Ditoro D. M., Member A. S. C. E., Paquin P. R., Subburamu K., and Gruber D. A. (1990) Sediment oxygen demand model: methane and ammonia oxidation. *J. Environ. Engin.* **116**, 945–986.
- Emerson S. and Hedges J. I. (1988) Processes controlling the organic carbon content of open ocean sediments. *Paleoceanography* **3**, 621–634.
- Emerson S., Jahnke R., Bender M., Froelich P., Klinkhammer G., Bowser C., and Setlock G. (1980) Early diagenesis in sediments from the eastern equatorial Pacific, 1. pore water nutrient and carbonate results. *Earth Planet. Sci. Lett.* **49**, 57–80.
- Emerson S., Fischer K., Reimers C., and Heggie D. (1985) Organic carbon dynamics and preservation in deep-sea sediments. *Deep-Sea Res.* **32**, 1–21.
- Fiadeiro M. E. and Veronis G. (1977) On weighted-mean schemes for the finite difference approximation to the advection-diffusion equation. *Tellus* **29**, 512–522.
- Froelich P. N., Klinkhammer G. P., Bender M. L., Luedtke N. A., Heath G. R., Cullen D., and Dauphin P. (1979) Early oxidation of organic matter in pelagic sediments of the eastern equatorial Atlantic: suboxic diagenesis. *Geochim. Cosmochim. Acta* **43**, 1075–1090.
- Goloway F. and Bender M. (1982) Diagenetic models of interstitial nitrate profiles in deep sea suboxic sediments. *Limnol. Oceanogr.* **27**, 624–638.
- Gratton Y., Edenborn H. M., Silverberg N., and Sundby B. (1990) A mathematical model for manganese diagenesis in bioturbated sediments. *Amer. J. Sci.* **290**, 246–262.
- Heggie D. T., Marais C., Hudson A., Dymond J., Beach R., and Cullen J. (1987) Organic carbon oxidation and preservation in NW Atlantic continental margin sediments. In *Geology and Geochemistry of Abyssal Plains* (ed. P. P. E. Weaver and J. Thomson), Vol. 31, pp. 215–236. Geological Society.
- Helder W. (1989) Early diagenesis and sediment-water exchange in the Savu Basin (Eastern Indonesia). *Netherlands J. Sea Res.* **24**, 555–572.
- Henrichs S. M. and Reeceburgh W. S. (1987) Anaerobic mineralization of marine sediment organic matter: rates and the role of anaerobic processes in the oceanic carbon economy. *Geomicrob. J.* **5**, 191–237.
- Honjo S., Manganini S., and J. J. Cole (1982) Sedimentation of biogenic matter in the deep ocean. *Deep-Sea Res.* **29**, 609–625.
- Humphrey A. E. (1972) The kinetics of biosystems: a review. In *Chemical Reactor Engineering* (ed. R. F. Gould); ACS Adv. Chem. Ser. **109**, pp. 630–650.
- Iversen N. and Jørgensen B. B. (1985) Anaerobic methane oxidation rates at the sulfate-methane transition in marine sediments from Kattegat and Skagerrak (Denmark). *Limnol. Oceanogr.* **30**, 944–955.
- Jahnke R. A. (1990) Early diagenesis and recycling of biogenic debris at the seafloor, Santa Monica Basin, California. *J. Mar. Res.* **48**, 413–436.
- Jahnke R. A., Emerson S. R., and Murray J. W. (1982) A model of oxygen reduction, denitrification, and organic matter mineralization in marine sediments. *Limnol. Oceanogr.* **27**, 610–623.
- Jahnke R. A., Emerson S. R., Cochran J. K., and Hirschberg D. J. (1986) Fine scale distributions of porosity and particulate excess ^{210}Pb , organic carbon and CaCO_3 in surface sediments of the deep equatorial Pacific. *Earth Planet. Sci. Lett.* **77**, 59–69.
- Jørgensen B. B. (1977) The sulphur cycle of a coastal marine sediment (Limfjorden, Denmark). *Limnol. Oceanogr.* **22**, 814–832.
- Jørgensen B. B. (1978) A comparison of methods for the quantification of bacterial sulfate reduction in coastal marine sediments. II. Calculations from mathematical models. *Geomicrobiol. J.* **1**, 29–47.
- Jørgensen B. B. (1983) Processes at the sediment-water interface. In *The Major Biogeochemical Cycles and Their Interactions* (ed. B. Bolin and R. B. Cook), pp. 477–509. Scope.
- Jørgensen B. B., Bang M., and Blackburn T. H. (1990) Anaerobic mineralization in marine sediments from the Baltic Sea-North Sea transition. *Mar. Ecol. Prog. Ser.* **59**, 39–54.
- Lampitt R. S. (1985) Evidence for the seasonal deposition of detritus to the deep-sea floor and its subsequent resuspension. *Deep-Sea Res.* **32**, 885–897.
- Li Y. H. and Gregory S. (1974) Diffusion of ions in sea water and in deep-sea sediments. *Geochim. Cosmochim. Acta* **38**, 703–714.
- Lochte K. and Turley C. M. (1988) Bacteria and cyanobacteria associated with phytodetritus in the deep sea. *Nature* **333**, 67–69.
- Martin W. R., Bender M., Leinen M., and Orchard J. (1991) Benthic organic carbon degradation and biogenic silica dissolution in the central equatorial Pacific. *Deep-Sea Res.* **38**, 1481–1516.
- Middelburg J. J. (1989) A simple rate model for organic matter decomposition in marine sediments. *Geochim. Cosmochim. Acta* **53**, 1577–1581.
- Middelburg J. J., Vlug T., and Van Der Nat F. J. W. A. (1993) Organic matter mineralization in marine systems. *Global Planet. Change* **8**, 47–58.
- Murray J. W. and Kuivila K. M. (1990) Organic matter diagenesis in the northeast Pacific: transition from aerobic red clay to suboxic hemipelagic sediments. *Deep-Sea Res.* **37**, 59–80.
- Pedersen T. F. and Price N. B. (1982) The geochemistry of manganese carbonate in Panama Basin sediments. *Geochim. Cosmochim. Acta* **46**, 59–68.
- Press W. H., Flannery B. P., Teukolsky S. A., and Vetterling W. T., eds. (1987) *Numerical Recipes. The Art of Scientific Computing*. Cambridge Univ. Press.
- Rabouille C. and Gaillard J. F. (1991a) A coupled model representing the deep-sea organic carbon mineralization and oxygen consumption in surficial sediments. *J. Geophys. Res.* **96**, 2761–2776.
- Rabouille C. and Gaillard J. F. (1991b) Towards the EDGE: Early diagenetic global explanation. A model depicting the early diagenesis of organic matter, O_2 , NO_3 , Mn and PO_4 . *Geochim. Cosmochim. Acta* **55**, 2511–2525.
- Reimers C. E. and Suess E. (1983) The partitioning of organic carbon fluxes and sedimentary organic matter decomposition rates in the ocean. *Mar. Chem.* **13**, 141–168.
- Reimers C. E., Jahnke R. A., and McCorkle D. C. (1992) Carbon fluxes and burial rates over the continental slope and rise off central California with implications for the global carbon cycle. *Global Biogeochem. Cyc.* **6**, 199–224.
- Revsbech N. P., Jørgensen B. B., and Blackburn T. H. (1980) Oxygen in the sea bottom measured with a microelectrode. *Science* **207**, 1355–1356.
- Roden E. E. and Tuttle J. H. (1993) Inorganic sulfur cycling in mid and lower Chesapeake Bay sediments. *Mar. Ecol. Prog. Ser.* **93**, 101–118.
- Rowe G. T. and Staresinic N. (1979) Sources of organic matter to the deep-sea benthos. *Ambio. Spec. Rep.* **6**, 19–23.
- Sarnthein M., Winn K., Duplessy J.-C., and Fontugne M. R. (1988) Global variations of surface ocean productivity in low and mid latitudes: influence on CO_2 reservoirs of the deep ocean and atmosphere during the last 21000 years. *Paleoceanography* **3**, 361–399.
- Sayles F. L., Martin W. R., and Deuser W. G. (1994) Response of benthic oxygen demand to particulate organic carbon supply in the deep sea near Bermuda. *Nature* **371**, 686–689.
- Smith K. L. J., Baldwin R. J., and Williams P. M. (1992) Reconciling particulate organic carbon flux and sediment community oxygen consumption in the deep North Pacific. *Nature* **359**, 313–316.
- Soetaert K., Herman P. M. J., and Middelburg J. (1996) Dynamic response of deep-sea sediments to seasonal variations: a model. *Limnol. Oceanogr.* (submitted).
- Thomann R. V. and Mueller J. A. (1987) *Principles of Surface Water Quality Modeling and Control*. Harper & Row.
- Tromp T. K., Van Cappellen P., and Key R. M. (1995) A global model for the early diagenesis of organic carbon and organic phosphorus in marine sediments. *Geochim. Cosmochim. Acta* **59**, 1259–1284.
- Ullman W. J. and Aller R. C. (1982) Diffusion coefficients in near-shore marine sediments. *Limnol. Oceanogr.* **27**, 552–556.
- Van Cappellen P. and Wang Y. (1995) Cycling of iron and manganese in surface sediments: A general early diagenetic model. *Amer. J. Sci.* (in press).
- Van Cappellen P., Gaillard J. F., and Rabouille C. (1993) Biogeo-

chemical transformations in sediments: kinetic models of early diagenesis. In *Interactions of C, N, P and S Biogeochemical Cycles and Global Change* (ed. R. Wollast et al.), pp. 401–446. Springer-Verlag.

Van Genuchten M. T. (1981) Analytical solutions for chemical transport with simultaneous adsorption, zero-order production and first-order decay. *J. Hydrol.* **49**, 213–233.

Walsh I. D. (1992) Large aggregate flux and fate at the seafloor: diagenesis during the rebound process. In *Deep-Sea Food Chains and the Global Carbon Cycle* (ed. G. T. Rowe and V. Pariente), pp. 365–374. Kluwer.

Westrich J. T. and Berner R. A. (1984) The role of sedimentary organic matter in bacterial sulfate reduction: the G-model tested. *Limnol. Oceanogr.* **29**, 236–249.

APPENDIX A. NUMERICAL APPROXIMATION OF THE TRANSPORT EQUATION

1. Transport Equation

The general diagenetic equation, describing the concentration changes as a function of time due to advection and mixing and biogeochemical reactions for dissolved substances is (Berner, 1980; Van Cappellen et al., 1993)

$$\frac{\partial \Phi C}{\partial t} = -\frac{\partial}{\partial x} \left[-\Phi D_{\text{sed}} \frac{\partial C}{\partial x} + w_{\infty} \Phi_{\infty} C \right] + \sum \Phi \text{REAC}, \quad (\text{A1})$$

where C = concentration of a dissolved substance ($\text{mass} \cdot \text{L}^{-3}$ liquid), ΦC is the concentration per volume of bulk sediment, x = depth into the sediment, positive downward (L), t = time (T), Φ = porosity of the sediment (volume of liquid per volume of bulk sediment, dimensionless), D_{sed} = bulk sediment diffusion coefficient ($\text{L}^2 \cdot \text{T}^{-1}$), w_{∞} = advection rate at depth ($\text{L} \cdot \text{T}^{-1}$), Φ_{∞} = porosity at depth (—), and REAC = all chemical and biological reactions of the substance ($\text{mass} \cdot \text{L}^{-3}$ liquid $\cdot \text{time}^{-1}$) as described in Table 3.

In case of adsorption of the solute, the equation used is (Berner, 1980a,b)

$$\frac{\partial \Phi C}{\partial t} = -\frac{\partial}{\partial x} \left[-\frac{\Phi D_{\text{sed}}}{(1+K)} \frac{\partial C}{\partial x} + w_{\infty} \Phi_{\infty} C \right] + \frac{\sum \Phi \text{REAC}}{(1+K)},$$

where K = adsorption coefficient (dimensionless).

The equation for solid substance is

$$\frac{\partial (1-\Phi)S}{\partial t} = -\frac{\partial}{\partial x} \left[-(1-\Phi)Db \frac{\partial S}{\partial x} + v_{\infty}(1-\Phi_{\infty})S \right] + \sum (1-\Phi)\text{REAC}, \quad (\text{A2})$$

where Db = biological dispersion coefficient or bioturbation coefficient ($\text{L}^2 \cdot \text{T}^{-1}$), S = concentration of the solid substance, expressed per volume of solid, $S(1-\Phi)$ is per volume of bulk sediment, v_{∞} = advection rate at depth ($\text{L} \cdot \text{T}^{-1}$), and intraphase mixing is assumed.

2. Boundary Conditions

At the lower boundary ($x = x_{\infty}$) it is assumed that the concentration of both dissolved and particulate substances does not change with depth (i.e., zero gradient):

$$\frac{dC}{dx} \Big|_{x=x_{\infty}} = \frac{dS}{dx} \Big|_{x=x_{\infty}} = 0.$$

For the upper boundary of dissolved substances ($x = 0$), the concentration in the middle of the layer immediately above the sediment-water interface C_{BW} is imposed:

$$C|_{x=0} = C_{\text{BW}}.$$

The upper boundary condition for solid substances is imposed as a flux F_S ($\text{mass} \cdot \text{L}^{-2} \cdot \text{T}^{-1}$):

$$F_S = -(1-\Phi_0)Db_0 \frac{dS}{dx} \Big|_{x=0} + (1-\Phi_{\infty})w_{\infty}S|_{x=0}, \quad (\text{A3})$$

where $S|_{x=0}$ is the concentration of the solid substance at the bottom-water interface.

3. Approximating the Derivatives for Advective and Dispersive Transport

The spatial derivatives of the partial differential equations are approximated by means of weighted finite differences which are second order accurate. The space variable x is discretized into N sediment layers of (unequal) thickness Δx and the concentration in the centre of each layer is modeled (Fig. 2).

Direct differencing of the transport term in Eqn. A1 results in the formula (Thomann and Mueller, 1987)

$$\frac{\partial C}{\partial t} \Big|_i = \frac{\partial}{\partial x} \Big|_i \left[\frac{\Phi D_{\text{sed}}}{\Phi_i} \frac{\partial C}{\partial x} \right] - \frac{w_{\infty} \Phi_{\infty}}{\Phi_i} \frac{\partial C}{\partial x} \Big|_i$$

$$\frac{\partial C}{\partial t} \Big|_i$$

$$= \frac{\left(\Phi D_{\text{sed}} \frac{\partial C}{\partial x} \right) \Big|_{i,i+1} - \left(\Phi D_{\text{sed}} \frac{\partial C}{\partial x} \right) \Big|_{i-1,i}}{\Phi_i \Delta x_i} - \frac{w_{\infty} \Phi_{\infty} (C_{i,i+1} - C_{i-1,i})}{\Phi_i \Delta x_i}$$

$i = 1, \dots, N$. The terms $\{i, i+1\}$ and $\{i-1, i\}$ denote the interfacial between layers i and $i+1$, between i and $i-1$ respectively; Δx_i is the thickness of layer i . The concentrations at the interface (e.g., $C_{i,i+1}$) are calculated as the weighted average of the adjacent concentrations (i.e., C_i and C_{i+1}).

Thus, for dissolved substances the difference equation becomes

$$\frac{dC_i}{dt} = \frac{\Phi_{i,i+1} D_{\text{sed},i+1} (C_{i+1} - C_i)}{\Phi_i \Delta x_{i,i+1} \Delta x_i}$$

$$- w_{\infty} \Phi_{\infty} \frac{\alpha_{i,i+1} C_i + (1 - \alpha_{i,i+1}) C_{i+1}}{\Phi_i \Delta x_i} \quad (\text{a})$$

$$- \frac{\Phi_{i-1,i} D_{\text{sed},i-1} (C_i - C_{i-1})}{\Phi_i \Delta x_{i-1,i} \Delta x_i}$$

$$+ w_{\infty} \Phi_{\infty} \frac{\alpha_{i-1,i} C_{i-1} + (1 - \alpha_{i-1,i}) C_i}{\Phi_i \Delta x_i} \quad (\text{b})$$

$i = 1, \dots, N$. $\Delta x_{i,i+1}$ is the distance from the centre of layer i towards the centre of layer $i+1$; $\Phi_{i,i+1}$ denotes the porosity at the interface of sediment layers i and $i+1$, $D_{\text{sed},i+1}$ the corresponding diffusion coefficient; $\alpha_{i,i+1}$ is a weighing coefficient used to interpolate the concentration between sediment slices i and $i+1$, i.e., in case of equally thick slices and linear interpolation, $\alpha_{i,i+1}$ equals 0.5. The weighing coefficient allows to adjust the numerical scheme to the predominant mode of transport, such that the scheme is stable and with the smallest amount of numerical dispersion (Thomann and Mueller, 1987). In order to reduce numerical dispersion, we used weighted differences all over; i.e., the concentration was calculated at the interface of the sediment slices i and $i+1$. When setting $\alpha_{i,i+1}$ equal to $(1 + \sigma_{i,i+1})/2$, with $\sigma_{i,i+1}$ a function of the Peclet number (Fiadeiro and Veronis, 1977), one obtains an unconditionally stable scheme, which was used by Boudreau (1995) for solid substances.

In this equation, the upper term (a) denotes concentration changes due to what comes into layer i from $i+1$, while the lower term (b) denotes changes due to what comes in from layer $i-1$.

For solid substances we obtain

$$\begin{aligned} \frac{dS_i}{dt} = & \frac{(1 - \Phi_{i,i+1})D_{b,i+1}(S_{i+1} - S_i)}{(1 - \Phi_i)\Delta x_{i,i+1}\Delta x_i} - w_z(1 - \Phi_z) \\ & \times \frac{\alpha_{i,i+1}S_i + (1 - \alpha_{i,i+1})S_{i+1}}{(1 - \Phi_i)\Delta x_i} - \frac{(1 - \Phi_{i-1,i})D_{b,i-1,i}(S_i - S_{i-1})}{(1 - \Phi_i)\Delta x_{i-1,i}\Delta x_i} \\ & + w_z(1 - \Phi_z) \frac{\alpha_{i-1,i}S_{i-1} + (1 - \alpha_{i-1,i})S_i}{(1 - \Phi_i)\Delta x_i}. \end{aligned}$$

The advantage of this numerical scheme, compared to the one used, e.g., by Rabouille and Gaillard (1991a,b) is that it can be used in an unequally spaced grid and the mass budget is fully closed: changes in mass in layer i due to input from $i + 1$ are given by multiplying the upper term (a) with $\phi_i^* \Delta x_i$:

$$\frac{\Phi_{i,i+1}D_{sed,i,i+1}(C_{i+1} - C_i)}{\Delta x_{i,i+1}} - w_z\Phi_z[\alpha_{i,i+1}C_i + (1 - \alpha_{i,i+1})C_{i+1}],$$

which is equal to total mass loss in layer $i + 1$ towards i .

The zero gradient lower boundary equation in the weighted finite difference approximation becomes

$$\frac{C_{N+1} - C_N}{\Delta x_{N,N+1}} = \frac{S_{N+1} - S_N}{\Delta x_{N,N+1}} = 0.$$

The upper boundary of dissolved substances is imposed as a bottomwater concentration at a distance $\Delta x_0/2$ above the sediment-water interface. As the concentration at the bottomwater interface is then calculated by linearly interpolating the bottomwater concentration and the concentration in the middle of the first model segment, this relates to a diffusive boundary layer of thickness $\Delta x_0/2$.

The rate of change of solids in the first sediment slice is determined by F_s , the flux to the sediment-water interface and what goes out to the underlying sediment slice:

$$\begin{aligned} \frac{dS_1}{dt} = & \frac{F_s}{(1 - \Phi_1)\Delta x_1} + \frac{(1 - \Phi_{1,2})D_{b,1,2}(S_2 - S_1)}{(1 - \Phi_1)\Delta x_{1,2}\Delta x_1} \\ & - w_z(1 - \Phi_z) \frac{\alpha_{1,2}S_1 + (1 - \alpha_{1,2})S_2}{(1 - \Phi_1)\Delta x_1}. \end{aligned}$$